Geoscience Frontiers 12 (2021) 101102

HOSTED BY

Contents lists available at ScienceDirect

Geoscience Frontiers

journal homepage: www.elsevier.com/locate/gsf

Research Paper

The Late Cretaceous source-to-sink system at the eastern margin of the Tibetan Plateau: Insights from the provenance of the Lanping Basin

Licheng Wang [a,*], Lijian Shen [b], Chenglin Liu [b], Ke Chen [c], Lin Ding [a], Chengshan Wang [d]

[a] CAS Center for Excellence in Tibetan Plateau Earth Sciences, Key Laboratory of Continental Collision and Plateau Uplift, Institute of Tibetan Plateau Research, Chinese Academy of Sciences, Beijing 100101, China
[b] MNR Key Laboratory of Metallogeny and Mineral Assessment, Institute of Mineral Resources, Chinese Academy of Geological Sciences, Beijing 100037, China
[c] Yunnan Geological Survey, Kunming 650051, China
[d] School of Earth Sciences and Resources, China University of Geosciences, Beijing 100083, China

ARTICLE INFO

Article history:
Received 8 June 2021
Received in revised form 26 August 2021
Accepted 4 November 2020
Available online 10 December 2020

Handling Editor: Christopher Spencer

Keywords:
Detrital Zircons
Drainage
Late Cretaceous
Source-to-sink
Lacustrine Basin
Tibetan Plateau

ABSTRACT

The surface uplift of the Tibetan Plateau (TP) and its geomorphology evolution has triggered aridification of Asia's interior and drainage development at the eastern margin of the plateau. However, how the pre-Cenozoic early growth histories of the TP impact the drainage system and climate is poorly constrained. The Late Mesozoic Lacustrine evaporite-bearing basins on the eastern margin of the TP record significant information on the uplift of the source terranes, source-to-sink system development and climate change. In this study, we presented detrital zircon U–Pb ages from the Upper Cretaceous Yunlong Formation in the Lanping Basin, as well as Hf isotopic, petrographic, direct statistical, and multidimensional scaling analyses, and use them to characterize the provenance and reconstruct the drainage system. All of the samples have five major age peaks at 200–290 Ma, 400–490 Ma, 750–1000 Ma, 1750–1950 Ma, and 2400–2600 Ma with mostly negative $\varepsilon_{Hf}(t)$ values (81%). We infer the sediments are primarily derived from recycled sediments of the Songpan-Garze terrane, and partly from the Sichuan Basin and the Southern Qiangtang terrane, as well as the exposed magmatic rocks of the Yidun Arc and Songpan-Garze terrane. The provenance features of the contemporaneous sediments from the Sichuan, Xichang, Chuxiong, and Simao basins indicate a complex hierarchical drainage pattern on the eastern margin of the TP during the Late Cretaceous. The hierarchical drainage system exhibits a complete gradational cycle of lake-basin types from overfilled freshwater Sichuan Basin through balanced fill saline Xichang Basin and underfilled hypersaline Chuxiong, Lanping, Simao, and Khorat Plateau basins from proximal to distal. The early growth of the TP primarily controlled the drainage and lake-basin evolution by not only causing the uplift and exhumation of the source areas and providing large amounts of clastic material to the proximal sub-drainage areas but also intensifying the aridity and deposition of evaporites.

1. Introduction

The surface uplift of the Tibetan Plateau (TP) has been a topic of great interest for several decades because it was not only related to aridification of Asia's interior but also triggered large-scale river reorganization and drainage evolution on the southeastern margin of the plateau (Raymo and Ruddiman, 1992; Clift et al., 2006; Dupont-Nivet et al., 2007; Wang et al., 2008; Ding et al., 2017). However, the pre-Cenozoic history of the TP is poorly understood. Recent advances in thermochronology have shown that rapid exhumation occurred during the Late Cretaceous from central Tibet (Rohrmann et al., 2012; Wang and Wei, 2013) to the eastern margin of the TP (Liu-Zeng et al., 2018; Liu et al., 2019), indicating that plateau growth began during the Late Cretaceous. The early growth of the TP, prior to the collision between India and Asia, significantly influenced the development of the drainage basins. A series of Mesozoic fluvial-lacustrine basins developed on the eastern margin of the TP, including the Sichuan, Xichang, Chuxiong, Lanping, Simao, and Khorat Plateau basins. A significant transformation of the sedimentary environments in most of these basins changed from fluvial in the Early Cretaceous to lacustrine in the Late Cretaceous (Wang et al., 2014b, 2020a; Deng et al., 2018; Li et al., 2018). Our recent study revealed that the paleo-Mekong River drained from the Songpan-Garze terrane and the Sichuan Basin to the Simao Basin during the late Early Cretaceous (Wang et al., 2020a), and indicated the provenance linkage between the Sichuan and Simao basins in the Late Cretaceous (Wang et al., 2014b). Deng et al. (2018) further proposed a transcontinental drainage system that flowed from the Sichuan Basin to the Xichang and Chuxiong basins and even to the Lanping-Simao Basin from the Late Cretaceous to the Early Paleogene. However, the

* Corresponding author.
E-mail address: lichengwang@itpcas.ac.cn (L. Wang).

https://doi.org/10.1016/j.gsf.2020.11.002

differences in the Late Cretaceous sedimentary sequences between the Sichuan-Xichang-Chuxiong basins and the Lanping-Simao basins (Wang et al., 2014b; Deng et al., 2018; Li et al., 2018; Liu et al., 2018) and the limit amount of detrital zircon (DZ) U–Pb age data for the Lanping-Simao basins (Wang et al., 2014b) result in the current source-to-sink scenario being simple and poorly constrained.

Lacustrine basin deposits are a downstream archive of larger drainage systems, and thus, they provide significant information on the geomorphological evolution and uplift processes that occurred in the source areas (Carroll et al., 2006). The Late Cretaceous lacustrine Lanping Basin provides a unique record that can be used to reconstruct the drainage and source-to-sink system. In this study, we present detrital zircon U–Pb ages and Hf isotopic results combined with petrology, direct statistical comparison, and multidimensional scaling (MDS) and use it to constrain the provenance and to obtain insights into the drainage system reconstruction and tectonic implications.

2. Regional geology

2.1. Geological setting

The Indosinian Orogeny in southwestern China and Southeast Asia is characterized by the collisions of many Gondwana-affinity terranes, which resulted in the final closure of the paleo-Tethyan Ocean from the Late Permian to the Early Triassic (Metcalfe, 2013). Several sutures and volcanic arcs are developed, e.g., the Ganzi-Litang suture, Jinshajiang-Ailaoshan and Song Ma sutures, Shuanghu suture, Changning-Menglian suture, Yidun Arc, Jomda-Weixi Arc, and Yunxian-Jinggu Arc (Figs. 1 and 2). The modern tectonic framework is driven by the collision between Asia and India at about 65 Ma (Ding et al., 2005), which caused the extrusion of the Simao and Indochina blocks (Tapponnier et al., 1982). The Simao Block is separated from the South China Block by the Jinshajiang-Ailaoshan and Song Ma sutures to the east, and from the Baoshan and Sibumasu blocks by the Lincang Batholith and Changning-Menglian suture to the west (Sone and Metcalfe, 2008; Metcalfe, 2011) (Fig. 1). It is connected with the Northern Qiangtang terrane to the north and the Indochina Block to the south. The Changning-Menglian Suture is believed to be a remnant of the main Paleo-Tethys oceanic crust (Zhong, 1998). The Early Paleozoic magmatic activity related to the subduction of the proto-Tethys oceanic crust (Mao et al., 2012) or the Paleo-Tethys back-arc basin (Wang et al., 2013a) and the voluminous Triassic intrusions related to the collision of the Simao and Baoshan-Sibumasu blocks outcrop along the suture (e.g., Hennig et al., 2009; Peng et al., 2013) (Fig. 2). Dispute as to whether the tectonic setting of the Jinshajiang-Ailaoshan-Song Ma Suture is a back-arc basin or a branch of the Paleo-Tethys Ocean continues (e.g., Pan et al., 1997; Mo et al., 1998; Zhong, 1998; Metcalfe, 2013; Wang et al., 2018b). Abundant Early Permian to Late Triassic magmatic rocks outcrop along the Simao Block (Wang et al., 2018b; Li et al., 2019, and references therein) (Fig. 2). The Triassic Jomda-Weixi Arc with bimodal volcanic suite was formed in an extensional setting due to the slab break-off of the Jinshajiang Ocean slab (Wang et al., 2014a). The Late Triassic Yidun Arc is situated between the Jinshajiang and Ganzi-Litang sutures and is the result of the subduction of paleo-Tethyan Ocean and subsequent continent-continent collision (Wang et al., 2018a). The Emeishan large igneous province (LIP) with main eruption phase of 257–260 Ma (Wang et al., 2020b) was proposed a mantle plume origin (Xu et al., 2008) (Fig. 2). In addition, the Neoproterozoic magmatic rocks in the western Yangtze Block (also called as Kangdian basement) are well exposed (Fig. 2).

2.2. Regional stratigraphy

The Lanping Basin is located on the northern part of the Simao Block and is part of the Sanjiang Tethyan realm (Hou et al., 2003). The Lanping Basin has an irregular form. It is ~350 km long (N–S), 50–100 km wide (E–W), and is connected to the Simao Basin to the south and the Cenozoic Jianchuan Basin to the east (Fig. 1). The Lanping Basin evolved from a remnant marine and marine-continental basin in the Triassic (Xue et al., 2007) into a continental rift basin during the Jurassic–Cretaceous (Qu et al., 1998; Liu, 2013; Wang et al., 2014b). The middle and upper Triassic strata recorded the change from a deep-water basin to a shallow water delta (Mou et al., 1999). The Lower Jurassic Yangjiang Formation (Fm.), the Middle Jurassic Huakaizuo Fm., and the Late Jurassic Bazhulu Fm. are mainly composed of red clastic rocks (Mou et al., 1999; Xue et al., 2007). The Lower Cretaceous is composed of red fluvial sandstone and mudstone and can be divided into three formations: in ascending order, the Jingxing, Nanxin, and Hutousi Fms. (BGMRY, 1996), which are unconformably overlain by the Late Cretaceous Yunlong Fm. and are correlated with the Lower Cretaceous in the Simao and Vientiane basins (Wang et al., 2020a). The Yunlong Fm. is mainly composed of lacustrine siltstones and mudstones with evaporites. It was previously regarded to be Paleocene in age based on an ostracoda assemblage of *Sinocypris-Parailyocypris-Eucypris* and Charophyta genera *Obtusochara-Peckichara-Gyrogona-Harrisichara-Stephanochara* (Shuai, 1987; BGMRY, 1990; Qu et al., 1998). The Yunlong Fm. is equivalent to the Mengyejing Fm. in the Simao Basin, and their lithology and stratigraphic successions are well correlated (BGMRY, 1996; Qu et al., 1998) (Fig. 3). Newly published SHRIMP U–Pb ages for tuff beds in the Mengyejing Fm. (110–100 Ma) (Wang et al., 2015) indicate that the Yunlong Fm. is at least Cretaceous in age. Thus, we argue that the depositional age of the Yunlong Fm. is likely Late Cretaceous and possibly extend to the Paleocene (Fig. 3).The overlying Guolang Fm. is dominated by lacustrine purple quartz sandstones, siltstones, and mudstones and was previously interpreted to be Early to middle Eocene in age based on ostracoda, including *Limnocythere yunlongenesis*, *Pinnocypris gibba* (BGMRY, 1990), while Zhang et al. (2010) and Gourbet et al. (2017) suggest a Paleocene age for it (Fig. 3). The unconformably overlying Baoxiangsi Fm. is mainly composed of red coarse sandstones and conglomerates and contains Late Eocene mammalian fauna (BGMRY, 1996). The Jinsichang Fm. contains Oligocene plant fossils and is dominated by alluvial conglomerates and sandstones (BGMRY, 1996). Gourbet et al. (2017) merged the Jinsichang and Baoxiangsi Fms. into a single formation, that is, the Baoxiangsi Fm., in the Jianchuan Basin and interpreted it to be Eocene in age.

2.3. Potential source areas

Potential source areas include the nearby fold and thrust belts and/or orogens, recycled sediments from pre-Late Cretaceous sedimentary rocks, and exposed magmatic rocks. Thus, we compiled many published detrital zircon U–Pb ages for the surrounding terranes (Figs. 2 and 4) and the magmatic rocks in Supplementary Table S1.

The Carboniferous to Upper Jurassic sedimentary sequences in the Northern Qiangtang terrane are extensive exposed and have DZ age peaks at ~254 Ma, ~548 Ma, ~800 Ma, 1800 Ma, and ~2500 Ma (Fig. 4) (Gehrels et al., 2011; Ding et al., 2013). The DZ ages of the Cambrian to Jurassic strata in the Southern Qiangtang terrane have two major peaks at ~250 Ma and ~1866 Ma, with subordinate peaks at ~550 Ma, ~800 Ma, 950 Ma, and ~2500 Ma (Fig. 4) (Gehrels et al., 2011; Ma et al., 2017, Ma et al., 2018a), which is only slightly different than those of the Northern Qiangtang terrane. The DZ age peaks of the Carboniferous-Triassic strata in the Lhasa terrane are characterized by a diagnostic peak at ~1170 Ma and minor peaks at ~560 Ma and ~1850 Ma (Fig. 4) (Zhu et al., 2011a; Li et al., 2014; Cai et al., 2016).

The DZs from the Triassic Yidun Group in the Yidun Arc terrane have peaks at ~240 Ma, ~446 Ma, ~996 Ma, ~1818 Ma, and ~2480 Ma (Fig. 4). The intensive magmatic activity at 230–193 Ma ($\varepsilon_{Hf}(t)$ values of −22.7 to 6.1) was related to the subduction of the Ganzi-Litang Ocean and the subsequent collision between the Yidun and Songpan-Garze terranes (Reid et al., 2007; He et al., 2013a; Peng et al., 2014; Cao et al., 2016; Wang et al., 2018a).

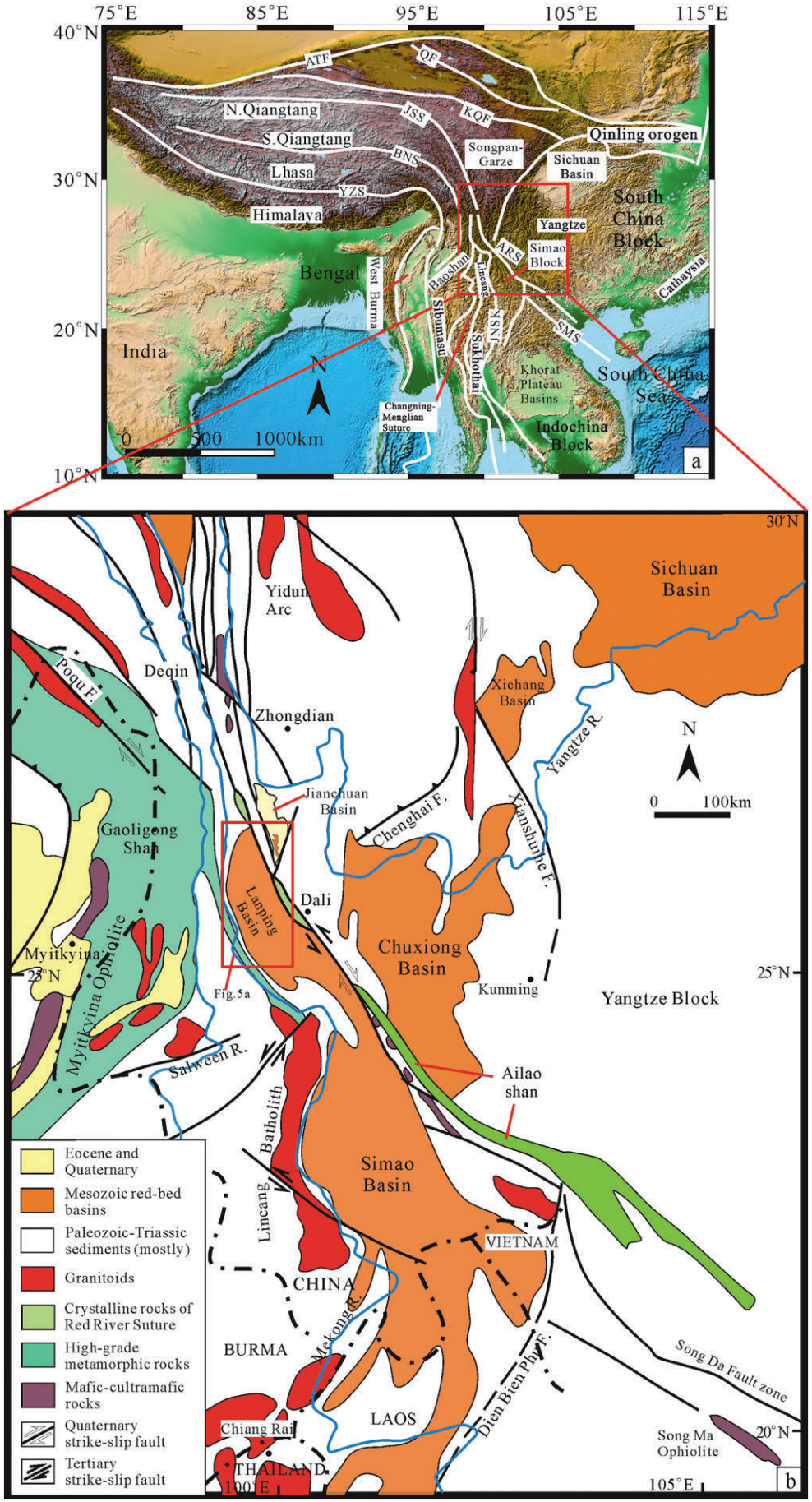

The DZ ages of the Songpan-Garze terrane are mainly grouped into five age populations of 2400–2500 Ma, 1850–1950 Ma, 750–900 Ma, 400–450 Ma, and 235–300 Ma (Fig. 4) (Weislogel et al., 2006; Ding et al., 2013). Late Triassic granitoids with ages ranging from 228 Ma to 197 Ma and $\varepsilon_{Hf}(t)$ values of −5.5 to 5.5 were extensively intruded into the Triassic turbidites (Roger et al., 2004; Zhang et al., 2006; Xiao et al., 2007; Cai et al., 2009, 2010; Yuan et al., 2010; Chen et al., 2017).

The metasedimentary basement rocks of the western Yangtze Block (Kangdian Basement) are widespread and include the Dahongshan Group (Greentree and Li, 2008), the Yanbian and Huili groups (Sun et al., 2009), the Dongchuan Group (Zhao et al., 2010), and the Kunyang Group (Wang et al., 2012). We compiled published DZ ages for the metasedimentary basement rocks and these DZs have major peaks at ~830 Ma, ~1850 Ma, and ~ 2460 Ma (Fig. 4). Extensive Neoproterozoic magmatic rocks with mostly positive $\varepsilon_{Hf}(t)$ values are well exposed (Zhou et al., 2006; Zhao et al., 2018). The magmatic activity related to the Emeishan LIP at ~260 Ma, positive $\varepsilon_{Hf}(t)$ values, was extensive in the western Yangtze Block (Xu et al., 2008).

The Sichuan Basin is located in the western part of the Yangtze Block and consists of a pre-Middle Triassic passive continental margin and Late Triassic to Cretaceous foreland basin sediments (Meng et al., 2005). These sediments yield DZ age peaks at ~250 Ma, ~430 Ma, ~810 Ma, ~1860 Ma, and ~ 2500 Ma (Li et al., 2016b, 2018; Zhu et al., 2017; Yan et al., 2019).

The DZs from the Ordovician to Silurian sedimentary rocks in the Simao Block have age peaks at ~1100 Ma, ~960 Ma, ~560 Ma, and 428–446 Ma (Wang et al., 2014d; Zhao et al., 2017). The Baoshan terrane is a northern extension of the Sibumasu Block and is comprised of Cambrian to Triassic sedimentary rocks (BGMRY, 1990). The DZs from these sediments are characterized by a dominant peak at ~930 Ma and subordinate peaks at ~560 Ma, ~1725 Ma, and ~2490 Ma (Li et al., 2015; Zhao et al., 2017; Xu et al., 2019; Song et al., 2020) (Fig. 4).

The Jinshajiang-Ailaoshan Suture belt is composed of Late Devonian to Early Carboniferous ophiolites (Jian et al., 2009a, 2009b). The DZ ages of the Silurian-Early Devonian sandstones in the Ailaoshan Suture yield major age groups of 430–450 Ma, 700–850 Ma, and 900–1200 Ma (Lai, 2012; Burrett et al., 2014; Xia et al., 2016). Abundant magmatic rocks related to the Indosinian orogeny are exposed, for example, the Jomda-Weixi volcanic arc (Zi et al., 2012, 2013; Wang et al., 2014a; Yang et al., 2014a, 2014b).

The Changning-Menglian Suture is comprised of ophiolites related to the paleo- or/and proto-Tethys ocean and has a wide range of ages from 471 Ma to 439 Ma (Wang et al., 2013a). Devonian to Triassic sedimentary rocks are distributed roughly within the belt, and their DZs have two dominant peaks at ~560 Ma and ~910 Ma (Fig. 4). The Late Triassic Lincang batholiths (mainly 230–212 Ma) intruded in the eastern part of the belt (Dong et al., 2013; Peng et al., 2013).

3. Samples and analytical methods

3.1. Measured sections of the Yunlong formation in the Lanping Basin

Usually, the Yunlong Formation can be divided into three parts. The lower part consists of conglomerates (clay gravel), mudstones, and siltstones with evaporites; the middle part mainly is comprised of siltstone and mudstone interbedded with fine-grain sandstones; the upper part is dominated by a sequence of carbonate-bearing fine-grain clastic rocks (BGMRY, 1990, 1996; Wang et al., 2015; Liu and Zhu, 2016) (Fig. 4b), recording a full cycle of fresh water to saline/ hypersaline water, then to fresh water lake evolution (Qu et al., 1998). These sedimentary characteristics of the Yunlong Formation can be easily distinguished from other formations.

The studied sections of the Yunlong Formation strata are located in Yangcen in the Jianchuan Basin (GPS: 26°28′49”N, 99°47′44″E), and in Hexi (GPS: 26°54′48”N, 99°20′46″E), Tangdeng (GPS: 25°59′34”N, 99°20′35″E), and Nuodeng (GPS: 25°55′3”N, 99°22′42″E) in the Lanping Basin (Fig. 5a). Due to heavily covered conditions in the Lanping Basin, all measured sections are short stratigraphic interval. The outcropped successions in Yangcen mainly consist of lacustrine fine-grained clastic rocks, including fine-grained sandstones, siltstones, and mudstones (Shen et al., 2015) (Figs. 5b and 6a). A very thin layer of marl is outcropped at the bottom of the section, which is interpreted to be the upper part of the Yunlong Formation (Shen et al., 2015) representing the late stage of saline lake evolution (Qu et al., 1998). The Hexi section is near the gypsum mine (Zhu et al., 2011b; Wang et al., 2014c) and mainly comprised of siltstones and mudstones intercalated with fine-grained sandstones (Figs. 5b and 6b), which are interpreted to be the result of lacustrine deposition (BGMRY, 1990; Zhu et al., 2011b). The sedimentary sequences in Hexi and Tangdeng have common lithological assemblages and thus we correlate the intervals with the middle part of the Yunlong Formation (6c). There is a long history of rock salt production from the Yunlong Formation in Nuodeng village. The hypersaline lacustrine strata exposed here consist of red mudstones, siltstones and conglomerate with clay gravel with vein-like gypsum cutting into the mudstones (Figs. 5b and 6d) (Qu et al., 1998; Wang et al., 2014c). Thus, we use this section to correlate with the lower part of the Yunlong Formation.

3.2. Sampling and methods

Ten fine-grained sandstone and siltstone samples from the Yunlong Formation were chosen for point-counts. Sample locations and lithology are shown in Fig. 5b. Based on the Gazzi-Dickinson method (Ingersoll et al., 1984), at least 400 grains were counted for each thin section using the maximum grid spacing. The crystals and grains of sand size that larger than 62.5 μm are classified in the category of crystal or grain rather than in the category of rock fragment (Ingersoll et al., 1984). Note that about 400 grains include the altered minerals and heavy minerals; matrix and cement are not counted. The results are presented in Supplementary Table S2.

Seven sandstone and siltstone samples from the Yunlong Formation were collected for U–Pb geochronology and in-situ Hf isotopic analysis. The rock samples were crushed and zircon grains were obtained via heavy liquid and magnetic separation. About 300 zircon grains were hand-picked and mounted in epoxy-resin, and then, they were polished and coated with gold. Cathodoluminescence (CL) images of the zircons were taken at Beijing GeoAnalysis Cooperation Limited. The U–Pb dating of the samples was performed using an Agilent 7500a ICP-MS coupled with a New Wave UP 193FX laser ablation system at the Key Laboratory of Continental Collision and Plateau Uplift, Institute of Tibetan Plateau Research, Chinese Academy of Sciences. The procedures used are described by Cai et al. (2012). At least 100 zircon grains for each sample were analyzed. Zircon GJ-1 (608.5 ± 0.4 Ma; Jackson et al., 2004) was used as primary external standard for the calibration of the U–Pb dating. Zircon 91500 (1065.4 ± 0.6 Ma, Wiedenbeck et al., 2004) was analyzed as a secondary as procedural monitor. An analysis protocol of every two standard zircons plus ten sample spots was followed to reduce instrument drift, i.e., GJ-1 + 91500 + 10 spots+ GJ-1 + 91500. The laser operation conditions bracket a repetition rate of 8 Hz, an energy density of ~8 J/cm^2, and a spot size of 30 μm. Each analysis incorporated with ~15–20 s gas blank acquisition and 40 s

Fig. 1. (a) Simplified geological map of Tibet and SE Asia (after Cai et al., 2017), ATF = Altyn Tagh Fault; QF = Qilian Fault; KQF = Kunlun-Qinling Fault; JSS = Jinshajiang Suture Zone; BNS = Bangong-Nujiang Suture Zone; YZS = Yarlung Zangbo Suture Zone; ARS = Ailaoshan-Red River Suture Zone; SMS = Song Ma Suture Zone; JNSK = Jinghong-Nan-Sra Kaeo Suture Zone. (b) Sketch geological map showing the location of the Lanping Basin in SE Asia (adapted from Leloup et al., 1995; Wintsch and Yeh, 2013).

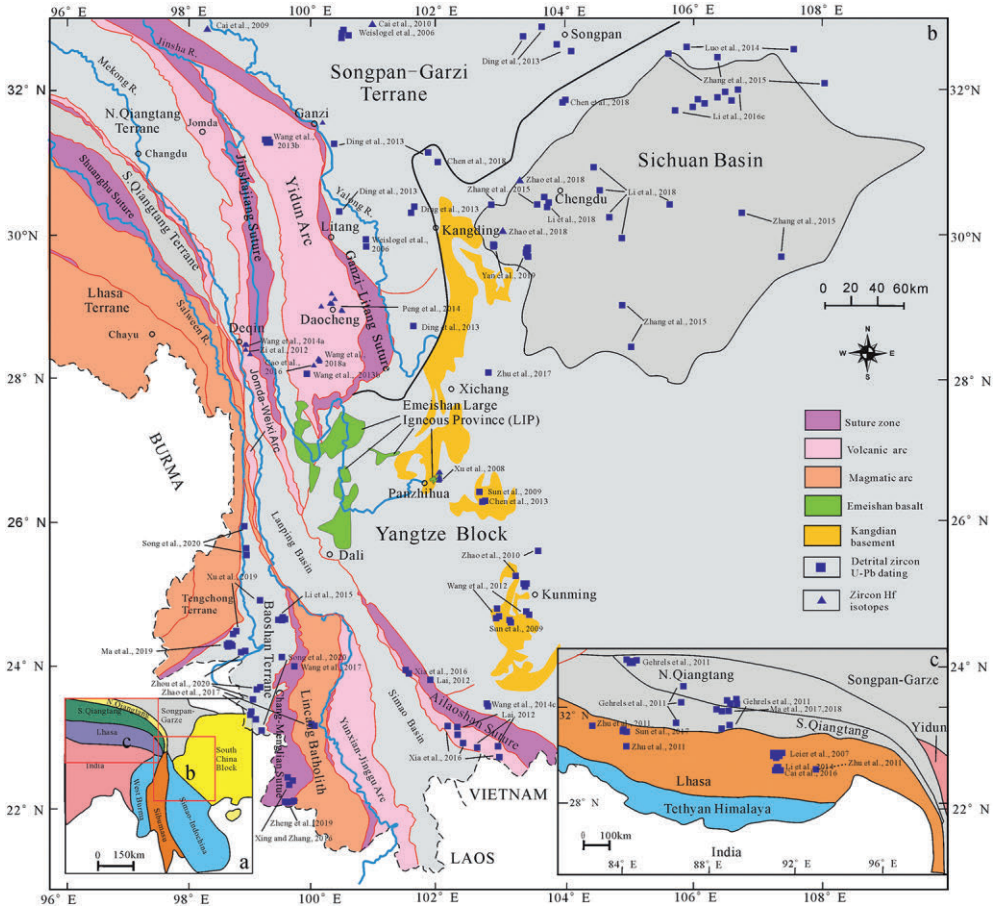

Fig. 2. (a) Distribution of major continental blocks and terranes in Southeast Asia (Modified from Metcalfe, 2013). Tectonic framework of the southeast Tibetan Plateau (b) and Tibetan Plateau (c) showing the major continental blocks, terranes, paleo-Tethys sutures, Emeishan large igneous province, and Kangdian basement which are the potential source regions for the Lanping Basin (modified from Zhu et al., 2011a, 2011b; Wang et al., 2014a; Yan et al., 2019). The compiled published sandstone samples with detrital zircon U—Pb ages and magmatic rock samples with Hf isotopic compositions are plotted. See the details in Supplementary Table S1.

Age		Lanping Basin	Thickness(m)	Lithology	Simao Basin	Environment
Paleogene	E_2b	Baoxiangsi Fm	800	Conglomerate, sandstone, sandy-mudstone	Mengla Fm	Braided river
	E_2g	Guolang Fm	500–800	Sandstone, siltstone interlcalated with mudstone	Denghei Fm	Lacustrine
	K_2-E_1y?	Yunlong Fm	266–800	Mudstone, siltstone, interlcalated evaporites	Mengyejing Fm	Hypersaline lake
Cretaceous	K_1h	Hutousi Fm	28–213	Sandstone	Pashahe Fm	Fluvial-paralic
	K_1n	Nanxing Fm	514–1960	Sandstone, siltstone	Mangang Fm	Meandering river
	K_1j	Jingxing Fm	412–1465	Silty-mudstone, sandstone	Jingxing Fm	Braided river
Jurassic	J_3b	Bazhulu Fm	83–1324	Mudstone interlcalated with fine-grained sandstone	Bazhulu Fm	Tidal flat
	J_2h	Huakaizuo Fm	118–1343	Sandstone sandy-mudstone, interlcalated with carbonate	Hepingxiang Fm	
	J_1y	Yangjiang Fm	64–2038	Sandy-mudstone	Zhangkezhai Fm	
Triassic	T_3m	Maichujing Fm	~1000	Sandy-mudstone, sandstone interlayered with mudstone	Manghuaihe Fm	Tidal delta

Fig. 3. Lithostratigraphy of the Lanping and Simao basins (data from BGMRY, 1990; Qu et al., 1998; Wang et al., 2015).

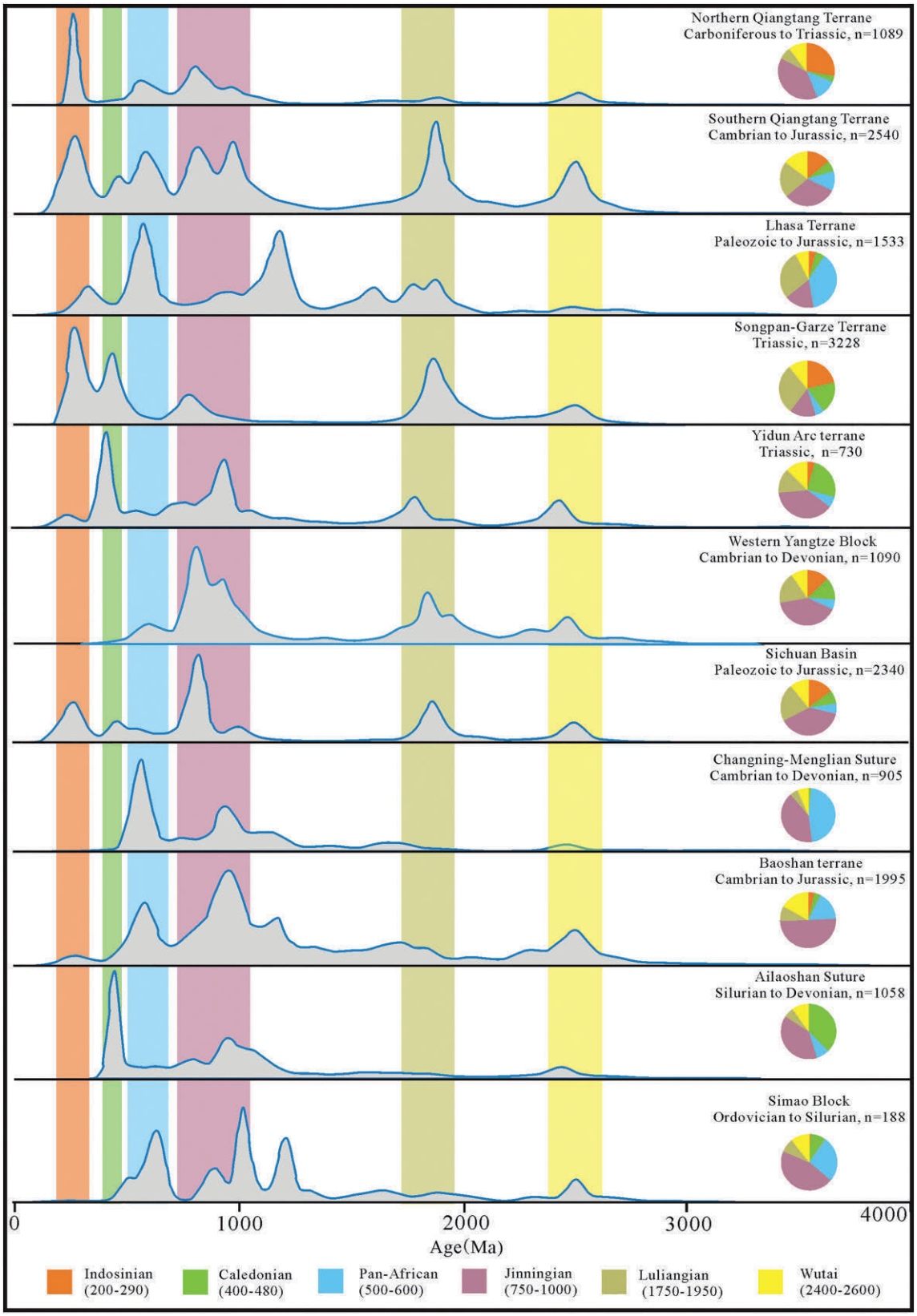

Fig. 4. Comparison of detrital zircon U—Pb Kernel Density Estimates (KDEs) plots of potential source terranes. KDEs are displayed for DZ ages with pie diagrams of six major age clusters: Indosinian 200–290 Ma; Caledonian 400–490 Ma; Pan-African 500–600 Ma; Grenville (Jinningian) 750–1000 Ma; Luliangian 1750–1950 Ma; Wutai 2400–2600 Ma. Data sources: Lhasa terrane (Paleozoic to Jurassic, Leier et al., 2007; Zhu et al., 2011a; Li et al., 2014; Cai et al., 2016; Sun et al., 2017); Northern Qiangtang terrane (Carboniferous to Triassic, Gehrels et al., 2011); Southern Qiangtang terrane (Cambrian to Jurassic, Gehrels et al., 2011; Ma et al., 2017; Ma et al., 2018a, 2018b); Yidun Arc terrane (Triassic, Wang et al., 2013b); Songpan-Garze terrane (Triassic, Weislogel et al., 2006; Ding et al., 2013); Sichuan Basin (Paleozoic to Jurassic, Luo et al., 2014; Li et al., 2016b, Li et al., 2018; Zhu et al., 2017; Yan et al., 2019); western Yangtze Block (Cambrian to Devonian, Sun et al., 2009; Zhao et al., 2010; Wang et al., 2012; Chen et al., 2013, 2018); Ailaoshan Suture (Silurian to Devonian, Lai, 2012; Xia et al., 2016); Simao Block (Ordovician to Silurian, Wang et al., 2014d; Zhao et al., 2017); Baoshan terrane (Cambrian to Jurassic, Li et al., 2015; Zhao et al., 2017; Ma et al., 2019; Xu et al., 2019; Song et al., 2020; Zhou et al., 2020); Changning-Menglian Suture (Cambrian to Devonian, Xing and Zhang, 2016; Wang et al., 2017; Zheng et al., 2019).

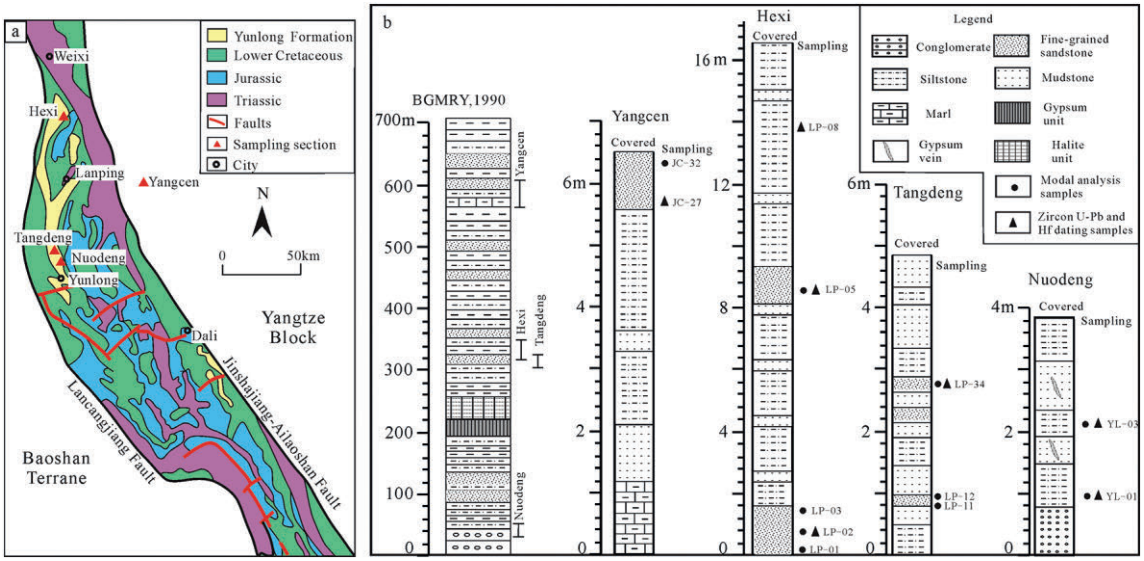

Fig. 5. (a) Simplified geological map of the Lanping Basin showing the locations of sampling sections (modified from Qu et al., 1998). (b) The lithostratigraphy of the type section of the Yunlong Formation in the Lanping Basin (BGMRY, 1990) and correlation between four measured short sections and the type section. See details in Section 3.1.

data acquisition from the sample ablation. About 45–55 s washout time by the spot sampling mode of the laser system occurs at the end of each analysis. The raw data was analyzed using Glitter V4.0. IsoplotR (Vermeesch, 2018a) was used to plot the KDEs (kernel density estimates, bandwidth = 30 Ma) diagrams. The best estimated ages are chosen based on the $^{206}Pb/^{238}U$ ratios of the <1000 Ma grains and on the $^{207}Pb/^{206}Pb$ ratios of the >1000 Ma grains (Pullen et al., 2008). Zircon ages with a concordance of 90%–110% were used.

The zircon Hf isotopic analyses were performed at Beijing GeoAnalysis Cooperation Limited using a Neptune plus MC-ICP-MS in combination with a Resolution SE 193 nm laser ablation system. The in-situ Hf isotope analysis was conducted on the same zones of the previously dated zircons. The instrument details and operation conditions are described by Hu et al. (2012). Zircon standard PLE was used as an external standard. The energy density of laser ablation used in this study was 7–8 J/cm^{-2}. A repetition rate of 10 Hz and a beam diameter of 38 μm was obtained. Helium was used as the carrier gas in the ablation cell. Each measurement consisted of 20s of acquisition of the background signal followed by 50 s of ablation signal acquisition. The directly obtained β_{Yb} value from the sample was applied to accurate correction of ^{176}Yb. The ratios of $^{179}Hf/^{177}Hf$ and $^{173}Yb/^{171}Yb$ were used to calculate the mass bias of Hf (β_{Hf}) and Yb (β_{Yb}). The data handling details are recorded in Wang et al. (2014b). The raw data was performed using ICPMSDataCal (Liu et al., 2010).

It is difficult to determine the true parent sources of the strata in a continental basin because the surrounding terranes, for example, an exhumed thrust-fold belt, a magmatic arc, a continental block, and recycled sediments, provide rock detritus to the basin, which mixes the parent information. Thus, dissimilarity quantification using statistical analysis was developed. In this study, the DZstats program (Saylor and Sundell, 2016) was used to conduct pairwise comparison (cross-correlation, likeness, similarity, the K–S test, and Kuiper's test) to create the straight statistic values. Multidimensional scaling (MDS) was employed to visualize the similarities (Vermeesch, 2013) using DZmds (Saylor et al., 2018). Samples with similar age distributions plot closer to each other than those of dissimilar age distributions (Vermeesch et al., 2016; Vermeesch, 2018a).

4. Results

4.1. Sandstone petrology

We analyzed ten sandstone samples from the Yunlong Formation. The detrital grains were mostly subangular to subrounded in morphology (Fig. 6). Quartz was the main clastic component (40%–67%). Monocrystalline grains were dominant with common secondary overgrowth. Feldspar constituted 13%–35% of the sand grains, indicating a felsic igneous source. The alkali feldspar content ranged from 53% to 62% of the total feldspar grains. The lithic fragments (17%–34%) mainly included the volcanic clasts. About 8%–21% of the total lithic fragments were metamorphic detritus consisting of quartzite, schist, and phyllite. The sedimentary lithic fragments consisted of mudstone, sandstone, and chert. The chert was most commonly polycrystalline quartz (e.g., Dickinson and Suczek, 1979); however, we grouped all of the chert grains in the lithic fragments following the method of Garzanti (2019). On the QFL and QmFLt diagrams (Fig. 7), all of the samples plot within the recycled orogen and dissected arc provenance fields, indicating that the sources are sedimentary and igneous rocks.

4.2. Zircon U–Pb isotopic ages

All of the detrital zircon U–Pb age data are presented in Supplementary Table S3. A total of 667 detrital zircon U–Pb ages with concordances of 90%–110% were for seven sandstone samples. Most of the grains (74%) were characterized by oscillatory zoning and Th/U ratios of >0.4, which indicates a magmatic origin (Supplementary Figs. S1 and S2). A few of the grains had low Th/U ratios of <0.1 and exhibited core-rim textures characteristic of a metamorphic origin.

Sample JC-27 was collected in the Yangcen area, Jianchuan Basin. Of the 100 analyses, 93 concordant ages yielded 3 major peaks at ~248 Ma (22%), ~832 Ma (22%), and ~1873 Ma (39%), with a minor peak at ~2429 Ma (7%) (Fig. 8).

For sample LP-02, 94 of the 101 single zircon ages were concordant. Most of the ages were clustered at ~1802 Ma (32%), ~276 Ma (19%),

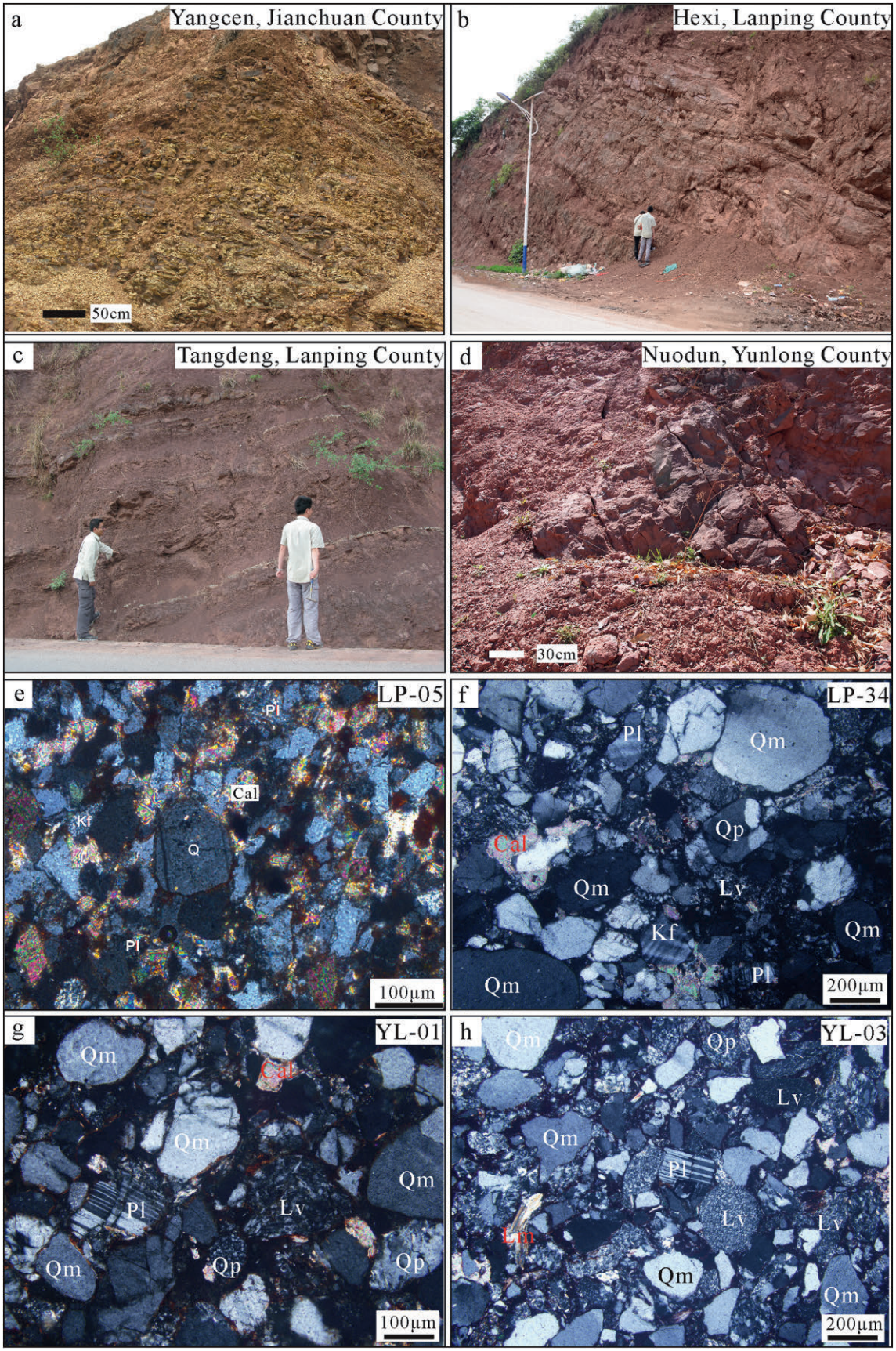

Fig. 6. (a–d) Field photographs of outcrops of the Yunlong Formation; (e) very fine-grained lithic-feldspathic sandstone (sample LP-05); (f) medium to fine-grained lithic-feldspathic sandstone (sample LP-34); (g, h) feldspatho-lithic sandstone (samples YL-01, YL-03).

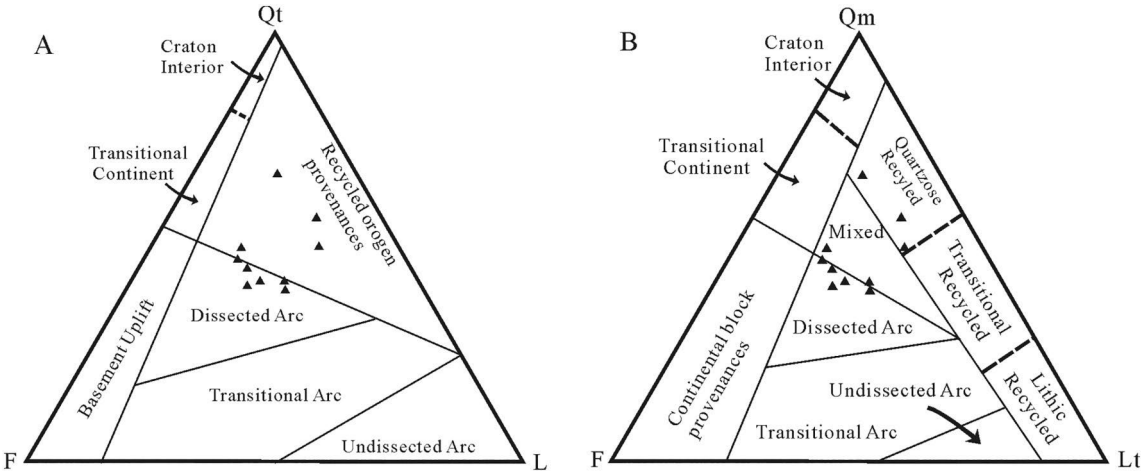

Fig. 7. QFL (a) and QmFLt (b) plots for framework modes of terrigenous sandstones showing provisional subdivisions according to inferred provenance type, modified from Dickinson et al. (1983). Qt = total quartz grains; Qm = quartz grains that are exclusively monocrystalline; F = total feldspar grains; L = total unstable lithic fragments; Lt = total polycrystalline lithic fragments.

and ~461 Ma (19%), with subordinate age peaks at ~840 Ma (16%) and ~2509 Ma (12%).

A total of 93 concordant ages out of the 104 analyses conducted on the zircons from sample LP-05 yielded two major peaks at ~284 Ma (31%) and ~426 Ma (33%) and two minor peaks at ~815 Ma (18%) and ~2461 Ma (10%).

For sample LP-08, 82 of the 100 single zircon ages were concordant. These ages yielded major peaks at ~276 Ma (25%) and ~1855 Ma (27%), with subordinate age peaks at ~454 Ma (13%), ~814 Ma (19%), and ~2488 Ma (10%).

For sample LP-34, 96 of the 102 single zircon ages were concordant. Most of the ages clustered at ~245 Ma (22%) and ~1879 Ma (31%), with minor peaks at ~435 Ma (13%), ~967 Ma (13%), and ~2517 Ma (17%).

A total of 102 concordant ages out of the 104 analyses conducted on the zircons from sample YL-01 yielded two major peaks at ~219 Ma (37%) and ~437 Ma (25%) and two minor peaks at ~761 Ma (18%) and ~1850 Ma (12%).

For sample YL-03, a total of 113 zircon grains were analyzed, and 107 concordant ages were obtained. The KDE diagram displays a significant peak at ~1863 Ma (38%) with three subordinate peaks at ~231 Ma (13%), ~428 Ma (14%), and ~975 Ma (23%) (Fig. 8).

4.3. Hf isotopes

A total of 109 zircon grains were analyzed to determine their in-situ Hf isotopic ratios. The results are presented in Supplementary Table S4. All of the samples exhibit a wide range of $\varepsilon_{Hf}(t)$ values between −24.7 and 11.26, with mostly (81%) being negative values (Fig. 9). For the 200–290 age cluster, most zircons have negative $\varepsilon_{Hf}(t)$ values. The $\varepsilon_{Hf}(t)$ values of the 400–490 Ma and 750–1000 Ma age cluster range from −13.25 to 4.6 and from −20.34 to 2.67, respectively. The ~1850 Ma age cluster has negative $\varepsilon_{Hf}(t)$ values and ~ 2500 Ma age cluster has slightly negative to positive $\varepsilon_{Hf}(t)$ values (−4.73 to 6.64).

4.4. Statistical comparison and multidimensional scaling (MDS) analysis

The first step to plot MDS map is to set consensus dissimilarity metrics. The most common used metrics are K–S and Kuiper tests (Vermeesch, 2018b). However, Wissink et al. (2018) argued that the metrics of likeness, similarity, and Kuiper test are more effective than the K–S test. Saylor and Sundell (2016) suggest that the cross-correlation have the best performance for sample with $n \geq 300$. In this study, the analyzed sample are $n = 100$ and compiled source region samples are $n > 300$. Thus, cross-correlation coefficients and Kuiper Test V values are considered as dissimilarities metrics and used for MDS plot (Fig. 10). All of the statistical comparison results are presented in Supplementary Table S5. The studied samples, all the compiled Late Cretaceous samples from the Lanping, Sichuan, Chuxiong, and Simao basins, and the compiled samples from the potential source terranes using both dissimilarity metrics were plotted (Fig. 10a–d). On the MDS plot (Fig. 10a, b), most studied samples are much closer to the Songpan-Garze terrane with higher cross-correlation coefficients (0.63–0.76) and lower Kuiper V values (0.19–0.31) than other potential source areas. Sample YL-03 is closer to the Southern Qiangtang terrane with the cross-correlation coefficient of 0.59 and Kuiper V value of 0.18. The Shepard plots show a lower stress in MDS plot with Kuiper V value than with cross-correlation coefficient (Fig. 10a, b). The coeval sediments of the Late Cretaceous in the Lanping, Simao, and Sichuan basins and Songpan-Garze terrane plot closely together and also close to the Sichuan Basin and Southern Qiangtang terrane, while the Upper Cretaceous in the Chuxiong Basin plot far apart (Fig. 10c, d).

5. Discussion

5.1. Provenance interpretation

The petrological observations indicate that the fine-grained sandstones and siltstones are rich in quartz with equally abundant feldspar and lithic fragments. They plot in recycled orogen and dissected arc fields (Figs. 6 and 7), which indicate sedimentary rock and igneous rock sources.

Several DZ age populations were identified for the studied samples: 200–290 Ma, 400–490 Ma, 750–1000 Ma, 1750–1950 Ma, and 2400–2600 Ma. These age populations are believed to be related to several tectonic and magmatic events or orogenies that occurred in China, that is, the Indosinian, Caledonian, Jinningian, Luliangian, and Wutai orogenies (Rogers and Santosh, 2002; He et al., 2013b). These age peaks overlap with the age distributions of the Songpan-Garze terrane, Sichuan Basin, and western Yangtze Block on the KDEs plots (Figs. 4 and 8) based on the following reasons: (1) Although the older zircons related to the Luliangian and Wutai orogenies could have been derived from most of the potential sources, the 1850–1880 Ma age population is very pronounced in most of the samples, but is absent or is not significant in the Northern Qiangtang terrane, the Changning-Menglian and Ailaoshan sutures, and the Simao Basin (Figs. 4 and 8); (2) the diagnostic age peak at ~1150 Ma is significant in the Lhasa terrane (Zhu et al.,

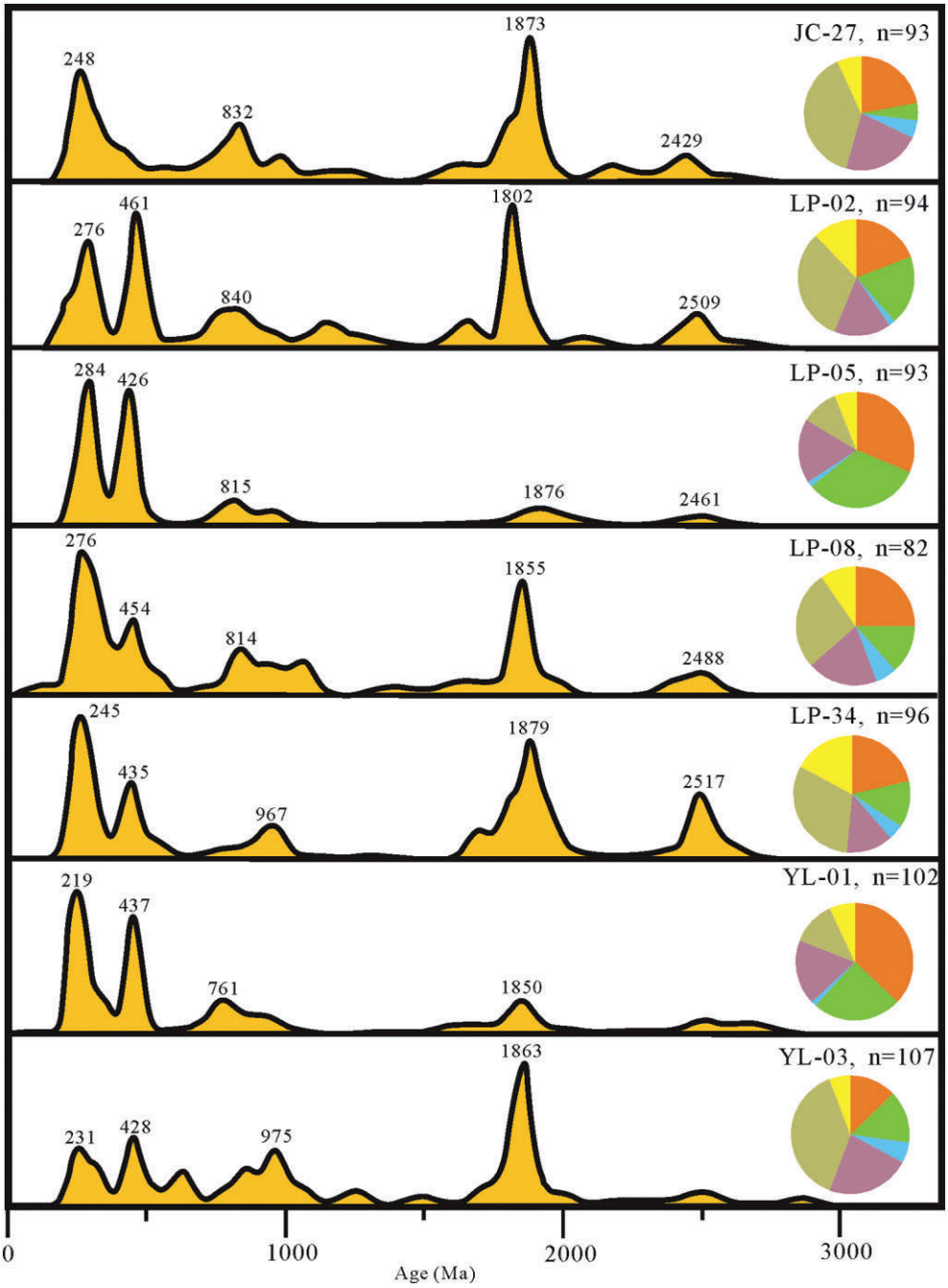

Fig. 8. Detrital zircon U—Pb ages showed as KDEs for the Upper Cretaceous Yunlong Formation sandstone samples, Lanping Basin.

2011a), but is absent in all of the samples (Fig. 8); (3) the 500–600 Ma age cluster with a peak at ~560 Ma, which is related to Pan-Africa orogeny, is significant in the age populations from the Southern Qiangtang terrane, the Lhasa terrane, the Baoshan terrane, the Simao Basin, and the Changning-Menglian Suture (Figs. 4 and 8), but is absent in the Lanping samples; (4) the Yidun Arc terrane is characterized by two major peaks at ~440 Ma and ~990 Ma, while the ~990 Ma age peak is absent in most studied samples; (5) the available zircon Hf data for the Triassic sediments of the Songpan-Garze terrane and the Sichuan Basin are characterized by mostly negative and slightly positive $\varepsilon_{Hf}(t)$ values (Zhang et al., 2014, Zhang et al., 2015). This is similar to the zircon $\varepsilon_{Hf}(t)$ values of the studied samples (Fig. 9). Moreover, the MDS plot indicate the most studied samples are much closer to the Songpan-Garze terrane (except sample YL-03). Note that the sample YL-03 has a subordinate peak at 975 Ma which is similar to those in the Southern Qiangtang terrane (Figs. 4 and 8) and plot closer to each other on the MDS plots (Fig. 10a, b). Nevertheless, the Late Cretaceous sediments in the Lanping, Simao, and Sichuan basins plot closer to the Songpan-Garze terrane, Southern Qiangtang terrane and Sichuan Basin (Fig. 10c, d).

The nearby exposed Permian to Triassic igneous rocks supplied detritus to the Yunlong Formation (Fig. 2) (Yang et al., 2014a). Most $\varepsilon_{Hf}(t)$ values for the U–Pb ages between 200 Ma and 290 Ma for the Yunlong Formation samples were negative with slightly positive values,

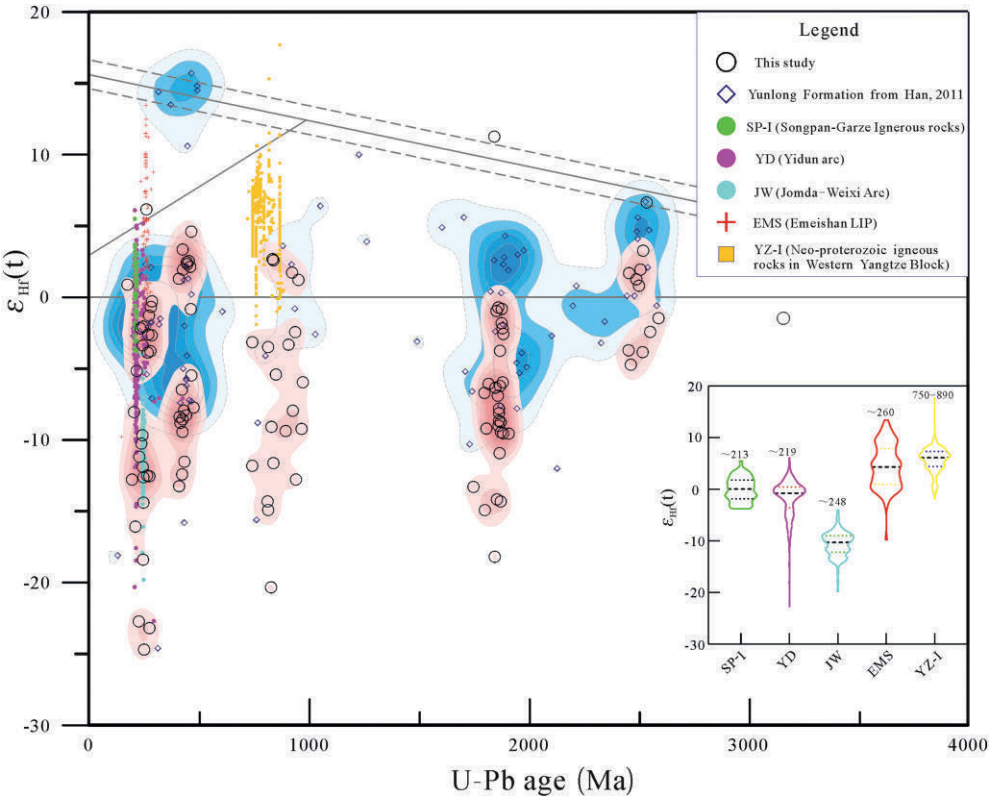

Fig. 9. Plot of $\varepsilon_{Hf}(t)$ values and ages from the magmatic rocks of the Jomda-Weixi Arc, Yidun Arc, Emeishan large igneous province, Songpan-Garze terrane, and Neoproterozoic igneous rocks in the western Yangtze Block (Kangdian Basement) using the Matlab code of Spencer et al. (2020). The violin plot clearly shows the major phases of the neighbored magmatic activities (Data from Xu et al., 2008; Cai et al., 2009, 2010; Zi et al., 2012; Peng et al., 2014; Wang et al., 2014a, 2018a; Cao et al., 2016; Zhao et al., 2018).

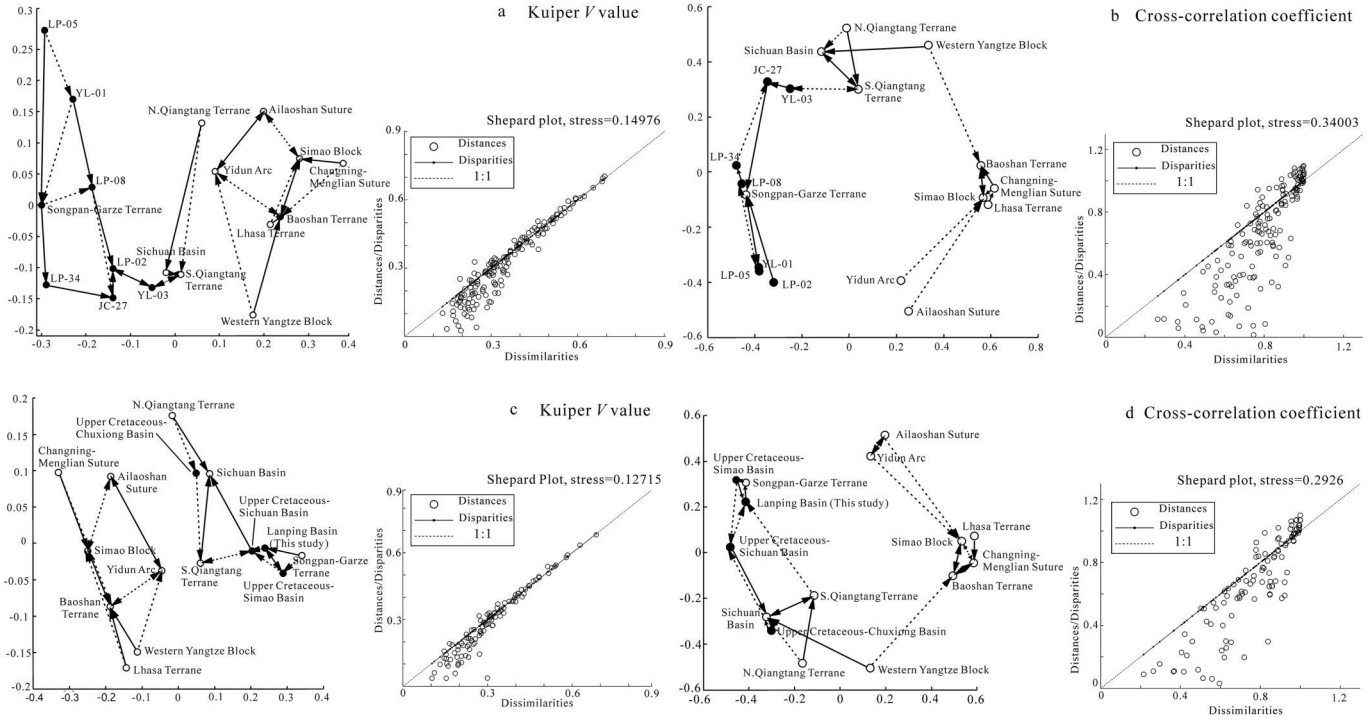

Fig. 10. Two dimensional multidimensional scaling (MDS) diagrams for (a, b) detrital zircon U—Pb ages of studied samples and compiled potential source areas and (c, d) compiled potential source areas and the Late Cretaceous sediments from the Lanping, Simao, Chuxiong, Sichuan basins. The MDS plots were constructed using DZmds (Saylor et al., 2018) with Kuiper Test *V* statistic (a, c) and cross-correlation coefficient (b, d). Solid and dash lines indicate strong and less strong relationship between samples and source areas, respectively. The Shepard plot shows the correlation between distance and dissimilarities where a good fit of MDS solution has a linear pattern and a low stress value. The DZ data of the Late Cretaceous sediments in the Simao, Sichuan, and Chuxiong basins are from Wang et al. (2014b), Deng et al. (2018), and Li et al. (2018).

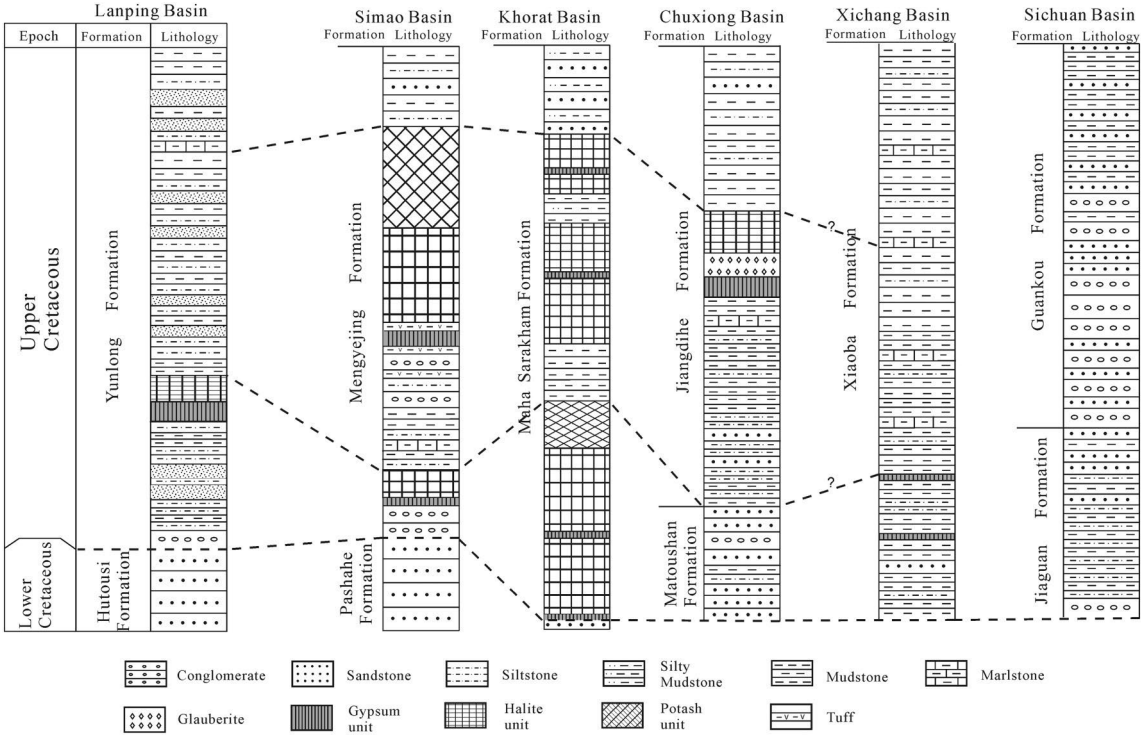

Fig. 11. Lithostratigraphic correlation of the Upper Cretaceous between the Lanping Basin and Simao, Chuxiong, Xichang, Sichuan, and Khorat Plateau basins. The classic stratigraphy in these basins are referred to BGMRY (1990), BGMRS (1991), El Tabakh et al. (1999), Wang et al. (2015), and Li et al. (2018).

while the $\varepsilon_{Hf}(t)$ values for U–Pb ages between 750 Ma and 890 Ma were more negative (Fig. 9), which is totally differ from the $\varepsilon_{Hf}(t)$ values of the Jomda-Weixi Arc, the Neoproterozoic igneous rocks and Emeishan LIP rocks. The Late Triassic Yidun Arc magmatic rocks (−22.7 to 6.1) (Peng et al., 2014; Cao et al., 2016; Wang et al., 2018a) and those of the Late Triassic granitoids in the Songpan-Garze terrane (−5.5 to 5.5) (Cai et al., 2009, 2010) are thus likely provided detritus to the Yunlong Formation. Based on the violin plot (Fig. 9), we argue that these magmatic rocks with main phase at 213–219 Ma are the sources of the sample YL-01.

Thus, we speculate that the samples from the Yunlong Formation are mostly recycled from the Songpan-Garze terrane and partly from the Sichuan Basin and the Southern Qiangtang terrane, together with magmatic rocks in the Yidun Arc and Songpan-Garze terrane. This provenance interpretation is supported by the following geological evidences: (i) The paleocurrent data indicates that the sediments of the Yunlong Formation mainly came from the northeast (NE) and northwest (NW) (Qu et al., 1998; Fan et al., 2010). The Southern Qiangtang terrane from NW and the Songpan-Garze terrane and Sichuan Basin from NE are consist with the paleocurrent. (ii) Previous heavy mineral assemblages demonstrate that the Yunlong Formation has a very low GTi index (most lower than 4%) and high ZTR (20%–25%) and ATi (mostly 30%–50%) indices (Zhu and Guo, 2017), indicating igneous source rocks with no contribution from the metamorphic rocks of the suture zones, which preclude the sources from the Jinshajiang-Ailaoshan and Changning-Menglian sutures. (iii) The contemporaneous sediments in the Sichuan Basin indicate a SW paleocurrent (Li et al., 2018) that flowed into the Xichang and Chuxiong basins (Deng et al., 2018). Thus, it is likely that the sources are from the Sichuan Basin and Songpan-Garze terrane. (iv) The Songpan-Garze terrane was likely exhumed as a denudation area since the Late Triassic (Yan et al., 2019) and further uplifted during the Early Cretaceous (~120 Ma) (Liu et al., 2019). The high topography and exhumation of the Songpan-Garze terrane thus provide detritus to adjacent basins. (v) The trans-continental paleo-Mekong River that flowed from Sichuan to Simao likely formed during the Early Cretaceous (Wang et al., 2020a) and connected the Sichuan and Lanping basins. Thus, we proposed that the Paleo-Mekong River drainage system possibly connected the sources and sinks.

5.2. Drainage reconstruction

In addition to the Lanping Basin, Late Cretaceous lacustrine sediments are found in the Sichuan, Xichang, Chuxiong, and Simao basins on the eastern margin of the TP (Fig. 1). During the Late Cretaceous, the tectonic compression of the Qinling Orogen spread to the Sichuan Basin and resulted in exhumation of the northern Sichuan Basin with southwestern tilting (Shen et al., 2007; Li et al., 2018). The southwestward paleocurrent that provided the detritus connected the Xichang and Chuxiong basins giving them similar provenance signatures and forming the paleo-Yangtze Basin (Deng et al., 2018). Previously studies depicted a drainage scenario that sediments sourced from Songpan-Garze terrane was transported to the Sichuan Basin, and then to the Xichang, Chuxiong, Lanping, Simao basins, and possibly Khorat Plateau basins by a transcontinental drainage system during the Late Cretaceous (Wang et al., 2014b; Deng et al., 2018). Actually, the source-to-sink system on the eastern margin of the TP during the Late Cretaceous most likely extended far beyond previous estimates. The scenarios may not simply indicate a paleo-large river and a downstream lake (Wang et al., 2014b; Deng et al., 2018) because several different types of lake developed. Moreover, the sedimentary environment and provenance of these basins varies significantly.

The Upper Cretaceous succession in the Sichuan Basin is mainly comprised of fluvial clastic rocks in the depocenter (Fig. 11) with interbedded red aeolian sandstones and hypersaline lacustrine evaporitic rocks on the southwestern margin (Li et al., 2016a; Deng et al., 2018;

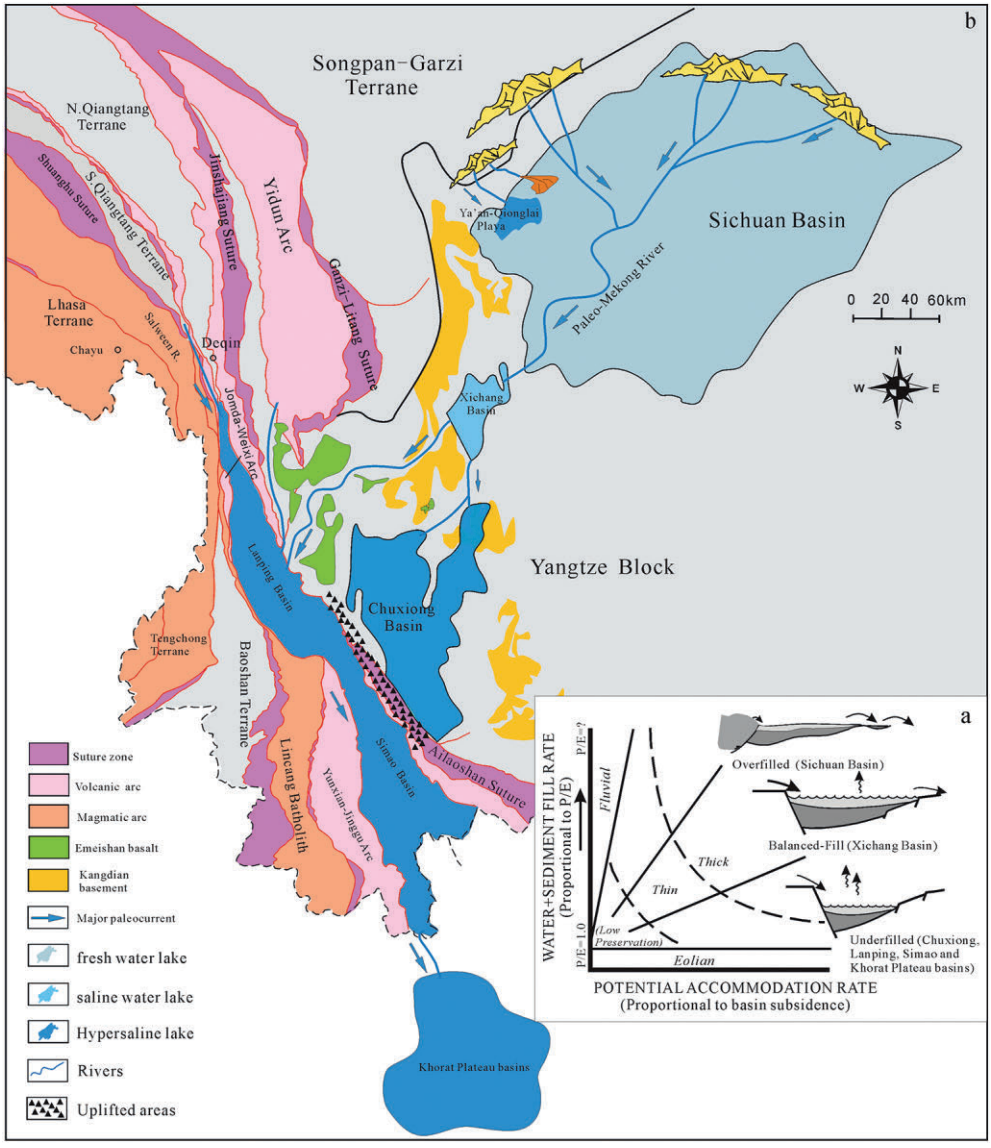

Fig. 12. (a) Reconstructions of drainage system at the eastern margin of the Tibetan Plateau during the Late Cretaceous (The paleogeographic configuration of the Sichuan and Lanping basins refer to Li et al., 2016a and Fan et al., 2010, respectively). (b) Illustrative lake basin type model recording a complete gradational cycle of lake-basin types from proximal to distal (modified from Carroll and Bohacs, 1999).

Liu et al., 2019). The provenance of the Sichuan Basin is mainly the Songpan-Garze terrane, the Longmenshan thrust belt, and the western Yangtze Block as well as the uplifted sediments of the northern and northeastern Sichuan Basin (Deng et al., 2018; Li et al., 2018). Thus, due to the high topography of the Songpan-Garze terrane since the Late Cretaceous (Liu et al., 2019), alluvial fans, fan-deltas, and mountain rivers developed on the SW margin of the Sichuan Basin with high sediment accumulation rates; while several braid rivers developed in the northern Sichuan Basin, which is consistent with the paleogeographic configuration (Li et al., 2016a, 2018). The fluvial-lacustrine facies association in the Sichuan Basin suggests an overfilled lake-basin based on Carroll and Bohacs (1999) (Fig. 12a). In contrast, the Upper Cretaceous in the Xichang and Chuxiong basins mainly consist of red sandstones, siltstones, and marls (Wang and Li, 1996) with interbedded gypsum-bearing mudstones in the Xichang Basin (BGMRS, 1991; Xu et al., 1997; Deng et al., 2018) and thick layers of rock salts, gypsum, and glauberites in the Chuxiong Basin (BGMRY, 1996) (Fig. 11). Thus the salinity of the Xichang Basin is much lower than that of the typical hypersaline Chuxiong Basin and the provenance is sourced from the uplifted northern Sichuan Basin (Deng et al., 2018). The facies associations of the Xichang Basin are fine-grained clastic rocks with thin layers of gypsum, indicating a deep water lake, and likely represent a balanced-fill saline lake-basin (Carroll and Bohacs, 1999) (Fig. 12a). We speculate that the provenance for the Chuxiong Basin is most likely the recycled uplifted sediments of the Sichuan Basin based on the MDS plot (Fig. 10c, d). The Upper Cretaceous in the Simao Basin is characterized by the fine-grained evaporite-bearing clastic rocks of the Mengyejing Fm. and is believed to have been deposited mainly in a hypersaline lake environment (Qu et al., 1998; Wang et al., 2014b), which is similar to that of the Lanping and Khorat Plateau basins. Thick evaporative facies associations were developed in the distal Chuxiong, Lanping, Simao, and Khorat Plateau basins indicating an underfilled lake-basin type (Carroll and Bohacs, 1999) (Fig. 12a). The Upper Cretaceous in Lanping, Simao, and Sichuan basins are mainly sourced from

the Songpan-Garze terrane, the Sichuan Basin, and the Southern Qiangtang terrane (Fig. 10c, d). While the provenance of the Upper Cretaceous in the Chuxiong Basin is much different from that of the equivalent sediments in the Lanping and Simao basins (Fig. 10c, d), and it did receive clastics from the Sichuan recycled sediments. Therefore, we suggest a complex hierarchical drainage pattern composed of two final sink center, several sub-drainages, and several sources. We propose that the Late Cretaceous drainage system on the eastern margin of the TP contained the paleo-Mekong River (Wang et al., 2020a), which drained from the Songpan-Garze terrane and the Sichuan Basin and drained southwestward; a small-scale hypersaline lake (Ya'an-Qionglai playa) on the southwestern margin of the Sichuan Basin, which formed due to the basin-bounding topographic highland (Li et al., 2016a); the fluvial-lacustrine and saline Xichang Basin; the hypersaline or playa Chuxiong, Lanping, and Simao lacustrine basins (Fig. 12b); and the hypersaline Khorat Plateau basins (Wang et al., 2014b; Deng et al., 2018). It should be noted that there is likely no hydrological connection between the Chuxiong and Lanping-Simao basins (Fig. 10c, d) although they have similar lithological associations. Their scenario is much more similar to that of the Oligocene to Miocene lakes of the Bangong-Nujiang Suture and the modern Siling Co drainage system in Central Tibet (Ma et al., 2018b). These lakes were in a hierarchical pattern with a drainage system and several sub-sinks and different salinity lakes coexist in the pattern.

5.3. Tectonic implications

The growth history of the Tibetan Plateau remains disputed, although many evidence had proposed different models to show the TP uplift ranging from Eocene, Oligocene, to Miocene (e.g., Chung et al., 1998; Rowley and Currie, 2006; Wang et al., 2008; Su et al., 2019, and references therein). However, the growth history prior to the collision of India and Asia remains poorly constrained. The plateau growth revealed by thermochronology began locally in central Tibet during the Late Cretaceous (Rohrmann et al., 2012). The low-temperature thermochronology data in the northern Sichuan Basin (Shen et al., 2007), in the Songpan-Garze terrane (Liu et al., 2019), and in Deqin and Weixi areas of the SE margin of the TP (Liu-Zeng et al., 2018) also revealed the fast cooling and exhumation during 120–80 Ma, which was related to the collision of the Lhasa and Qiangtang terranes (Liu-Zeng et al., 2018; Liu et al., 2019). The exhumation from these low-temperature thermochronometric data reveals the tectonic activities during the middle to late Cretaceous (120–80 Ma). The residual topography (120–80 Ma) from terrane accretion and continental collision have contributed to regionally high topography (Liu-Zeng et al., 2018). The high topography in the Songpan-Garze terrane may indicate the proto-plateau in central Tibet had extended to eastern margin of the TP during 120–80 Ma. The Late Cretaceous sediments in the Lanping, Simao, and Sichuan basins are sourced from the Songpan-Garze terrane further indicates a high topography at the eastern margin of the TP. We speculated that the middle to late Cretaceous tectonism and high topography likely controlled the development of the paleo-lake and drainage system. First, the tectonism caused the further uplift and exhumation of the source terranes and increased the detritus supply of the basin. Large amounts of clastics from the exhumed rocks of the Songpan-Garze terrane and the northern Sichuan Basin drained into the southwestern part of the Sichuan Basin (Li et al., 2016a). Thus, the lake evolution of the Late Cretaceous basins from overfilled to underfilled recorded a complete gradational cycle of lake basin types from proximal to distal that controlled by the early growth of the TP. Second, the uplift of the source terranes by tectonics blocked the atmospheric circulation and intensified the aridity (Li et al., 2018; Liu et al., 2019), causing the deposition of thick evaporites and aeolian sandstones in these basins. However, this only works on a small-scale in hydrologically closed basins (Ma et al., 2018a, 2018b) because the lake may range from freshwater or brackish to hypersaline within one climatic zone (Carroll and Bohacs, 1999). Thus, hypersaline water lakes only developed in the Ya'an-Qionglai areas in the SW Sichuan Basin, while most parts of the Sichuan and Xichang basins contained fresh to saline water lakes. The mid-Cretaceous marine incursion and subsequent regression (Wang et al., 2015) which is primarily controlled by global tectonics reduced the moisture content and could be another cause for thick evaporites of the hypersaline Lanping and Simao basins.

6. Conclusions

(1) Our detrital zircon U–Pb ages from the Upper Cretaceous Yunlong Formation in the Lanping Basin together with numerous published DZ ages for potential sources indicate that the sediments are primarily derived from recycled sediments of the Songpan-Garze terrane, and partly from the Sichuan Basin and the Southern Qiangtang terrane, as well as the exposed magmatic rocks of the Yidun Arc and Songpan-Garze terrane.
(2) The complex hierarchical drainage pattern on the eastern margin of the TP during the Late Cretaceous was comprised of the paleo-Mekong River, the small-scale hypersaline Ya'an-Qionglai playa, the saline Xichang Basin, the hypersaline or playa Chuxiong, Lanping, and Simao lacustrine basins, and the hypersaline Khorat Plateau basins, indicating a complete gradational cycle of lake-basin type from overfilled (Sichuan Basin) to balanced fill (Xichang Basin) and underfilled (Chuxiong, Lanping, and Simao basins).
(3) The early growth of the TP primarily controlled the source-to-sink system and lake-basin evolution by not only causing the uplift and exhumation of the source areas and providing large amounts of clastics to proximal sub-drainage areas but also intensifying the aridity and deposition of evaporites.

Supplementary data to this article can be found online at https://doi.org/10.1016/j.gsf.2020.11.002.

Declaration of Competing Interest

The authors declare that they have no known competing financial interests or personal relationships that could have appeared to influence the work reported in this paper.

Acknowledgments

This research was financially supported by the National Natural Science Foundation of China (Grant Nos. 41572067, 91855104, 41802111), the Strategic Priority Research Program of Chinese Academy of Sciences (Grant No. XDA 20170301), and the National Key Project for Basic Research of China (Grant No. 2011CB403007). We appreciate journal editor and two anonymous reviewers' detailed and constructive comments. We thank Dr. Yahui Yue for her assistance with the U–Pb dating analyses and LetPub (www.letpub.com) for its linguistic assistance during the preparation of this manuscript.

References

Bureau of Geology and Mineral Resources of Sichuan province (BGMRS), 1991. Regional Geology of Sichuan Province. Geological Publishing House, Beijing, pp. 1–735 (in Chinese).
Bureau of Geology and Mineral Resources of Yunnan province (BGMRY), 1990. Regional geology of Yunnan province. Geological Publishing House, Beijing, pp. 236–239 (in Chinese).
Bureau of Geology and Mineral Resources of Yunnan province (BGMRY), 1996. Stratigraphy (Lithostratic) of Yunnan province. China University of Geosciences Press, Wuhan, pp. 240–242 (in Chinese).
Burrett, C., Zaw, K., Meffre, S., Lai, C.K., Khositanont, S., Chaodumrong, P., Udchachon, M., Ekins, S., Halpin, J., 2014. The configuration of Greater Gondwana-evidence from LA-ICPMS, U-Pb geochronology of detrital zircons from the Palaeozoic and Mesozoic of

Southeast Asia and China. Gondwana Res. 26, 31–51. https://doi.org/10.1016/j.gr.2013.05.020.
Cai, H., Zhang, H., Xu, W., 2009. U-Pb zircon ages, geochemical and Sr-Nd-Hf isotopic compositions of granitoids in Western Songpan-Garze Fold Belt: petrogenesis and implication for tectonic evolution. J. Earth Sci. 20, 681–698. https://doi.org/10.1007/s12583-009-0054-8.
Cai, H., Zhang, H., Xu, W., Shi, Z., Yuan, H., 2010. Petrogenesis of Indosinian volcanic rocks in Songpan-Garze fold belt of the northeastern Tibetan Plateau: New evidence for Lithospheric delamination. Sci. China Earth Sci. 53, 1316–1328. https://doi.org/10.1007/s11430-010-4033-9.
Cai, F.L., Ding, L., Leary, R.J., Wang, H.Q., Xu, Q., Zhang, L.Y., 2012. Tectonostratigraphy and provenance of an accretionary complex within the Yarlung–Zangpo suture zone, southern Tibet: insights into subduction–accretion processes in the Neo–Tethys. Tectonophysics 574–575, 181–192.
Cai, F., Ding, L., Laskowski, A.K., Kapp, P., Wang, H., Xu, Q., Zhang, L., 2016. Late Triassic paleogeographic reconstruction along the Neo-Tethyan Ocean margins, southern Tibet. Earth Planet. Sci. Lett. 435, 105–114. https://doi.org/10.1016/j.epsl.2015.12.027.
Cai, F., Ding, L., Yao, W., Laskowski, A.K., Xu, Q., Zhang, J.E., Sein, K., 2017. Provenance and tectonic evolution of lower Paleozoic-Upper Mesozoic strata from Sibumasu terrane, Myanmar. Gondwana Res. 41, 325–336. https://doi.org/10.1016/j.gr.2015.03.005.
Cao, K., Xu, J.F., Chen, J.L., Huang, X.X., Ren, J.B., Zhao, X.D., Liu, Z.X., 2016. Double-layer structure of the crust beneath the Zhongdian arc, SW China: U–Pb geochronology and Hf isotope evidence. J. Asian Earth Sci. 115, 455–467. https://doi.org/10.1016/j.jseaes.2015.10.024.
Carroll, A.R., Bohacs, K.M., 1999. Stratigraphic classification of ancient lakes: balancing tectonic and climatic controls. Geology 27, 99–102.
Carroll, A.R., Chetel, L.M., Smith, M.E., 2006. Feast to famine: sediment supply control on Laramide basin fill. Geology 34, 197–200.
Chen, W.T., Zhou, M.F., Zhao, X.F., 2013. Late Paleoproterozoic sedimentary and mafic rocks in the Hekou area, SW China: Implication for the reconstruction of the Yangtze Block in Columbia. Precambrian Res. 231, 61–77. https://doi.org/10.1016/j.precamres.2013.03.011.
Chen, Q., Sun, M., Zhao, G., Yang, F., Long, X., Li, J., Wang, J., Yu, Y., 2017. Origin of the mafic microgranular enclaves (MMEs) and their host granitoids from the Tagong pluton in Songpan-Ganze terrane: an igneous response to the closure of the Paleo-Tethys Ocean. Lithos 290-291, 1–17. https://doi.org/10.1016/j.lithos.2017.07.019.
Chen, Q., Sun, M., Long, X., Zhao, G., Wang, J., Yu, Y., Yuan, C., 2018. Provenance study for the Paleozoic sedimentary rocks from the West Yangtze Block: Constraint on possible link of South China to the Gondwana supercontinent reconstruction. Precambrian Res. 309, 271–289. https://doi.org/10.1016/j.precamres.2017.01.022.
Chung, S.L., Lo, C.H., Lee, T.Y., Zhang, Y., Xie, Y., Li, X., Wang, K.L., Wang, P.L., 1998. Diachronous uplift of the Tibetan plateau starting 40? Myr ago. Nature 394, 769–773.
Clift, P.D., Blusztajn, J., Duc, N.A., 2006. Large-scale drainage capture and surface uplift in eastern Tibet-SW China before 24 Ma inferred from sediments of the Hanoi Basin, Vietnam. Geophys. Res. Lett. 33. https://doi.org/10.1029/2006gl027772 L19403.
Deng, B., Chew, D., Jiang, L., Mark, C., Cogné, N., Wang, Z., Liu, S., 2018. Heavy mineral analysis and detrital U-Pb ages of the intracontinental Paleo-Yangzte basin: Implications for a transcontinental source-to-sink system during late cretaceous time. Geol. Soc. Am. Bull. 130, 2087–2109. https://doi.org/10.1130/b32037.1.
Dickinson, W.R., Suczek, C., 1979. Plate tectonics and sandstone composition. Am. Assoc. Pet. Geol. Bull. 63, 2164–2182.
Dickinson, W.R., Beard, L.S., Brakenridge, G.R., Erjavec, J.L., Ferguson, R.C., Inman, K.F., Knepp, R.A., Lindberg, F.A., Ryberg, P.T., 1983. Provenance of north American Phanerozoic sandstones in relation to tectonic setting. Geol. Soc. Am. Bull. 94, 222–235.
Ding, L., Kapp, P., Wan, X., 2005. Paleocene–Eocene record of ophiolite obduction and initial India–Asia collision, south Central Tibet. Tectonics 24 (3). https://doi.org/10.1029/2004TC001729 TC3001.
Ding, L., Yang, D., Cai, F.L., Pullen, A., Kapp, P., Gehrels, G.E., Zhang, L.Y., Zhang, Q.H., Lai, Q.Z., Yue, Y.H., Shi, R.D., 2013. Provenance analysis of the Mesozoic Hoh-Xil-Songpan-Ganzi turbidites in northern Tibet: Implications for the tectonic evolution of the eastern Paleo-Tethys Ocean. Tectonics 32, 34–48. https://doi.org/10.1002/tect.20013.
Ding, L., Spicer, R.A., Yang, J., Xu, Q., Cai, F., Li, S., Mehrotra, R.C., 2017. Quantifying the rise of the Himalaya orogen and implications for the south Asian monsoon. Geology 45 (3), 215–218.
Dong, G.C., Mo, X.X., Zhao, Z.D., Zhu, D.C., Goodman, R.C., Kong, H.L., Wang, S., 2013. Zircon U-Pb dating and the petrological and geochemical constraints on Lincang granite in Western Yunnan, China: implications for the closure of the Paleotethys Ocean. J. Asian Earth Sci. 62, 282–294.
Dupont-Nivet, G., Krijgsman, W., Langereis, C.G., Abels, H.A., Dai, S., Fang, X.M., 2007. Tibetan plateau aridification linked to global cooling at the Eocene–Oligocene transition. Nature 445 (7128), 635–638.
El Tabakh, M., Utha-Aroon, C., Schreiber, B.C., 1999. Sedimentology of the cretaceous Maha Sarakham evaporites in the Khorat Plateau of northeastern Thailand. Sediment. Geol. 123, 31–62.
Fan, Y., Chen, H.D., Hou, Z.J., Lin, L.B., Luo, Y., Lv, D., 2010. The Paleogene tectonic sequence analysis based on the charactersitics of lithofacies and paleogeography in Lanping Basin, Yunnan. J. Stratigr. 31, 381–388 (in Chinese with English abstract).
Garzanti, E., 2019. Petrographic classification of sand and sandstone. Earth Sci. Rev. 192, 545–563. https://doi.org/10.1016/j.earscirev.2018.12.014.
Gehrels, G., Kapp, P., DeCelles, P., Pullen, A., Blakey, R., Weislogel, A., Ding, L., Guynn, J., Martin, A., McQuarrie, N., Yin, A., 2011. Detrital zircon geochronology of pre-Tertiary strata in the Tibetan-Himalayan orogen. Tectonics 30. https://doi.org/10.1029/2011tc002868 TC5016.
Gourbet, L., Leloup, P.H., Paquette, J.L., Sorrel, P., Maheo, G., Wang, G., Xu, Y.D., Cao, K., Antoine, P., Eymard, I., Liu, W., Lu, H.J., Replumaz, A., Chevalier, M., Zhang, K.X., Wu, J., Shen, T.Y., 2017. Reappraisal of the Jianchuan Cenozoic basin stratigraphy and its implications on the SE Tibetan plateau evolution. Tectonophysics 700, 162–179. https://doi.org/10.1016/j.tecto.2017.02.007.
Greentree, M.R., Li, Z., 2008. The oldest known rocks in South–Western China: SHRIMP U–Pb magmatic crystallisation age and detrital provenance analysis of the Paleoproterozoic Dahongshan Group. J. Asian Earth Sci. 33, 289–302.
He, D.F., Zhu, W.G., Zhong, H., Ren, T., Bai, Z.J., Fan, H.P., 2013a. Zircon U–Pb geochronology and elemental and Sr–Nd–Hf isotopic geochemistry of the Daocheng granitic pluton from the Yidun Arc, SW China. J. Asian Earth Sci. 67-68, 1–17. https://doi.org/10.1016/j.jseaes.2013.02.002.
He, M., Zheng, H., Clift, P.D., 2013b. Zircon U–Pb geochronology and Hf isotope data from the Yangtze River sands: Implications for major magmatic events and crustal evolution in Central China. Chem. Geol. 360, 186–203. https://doi.org/10.1016/j.chemgeo.2013.10.020.
Hennig, D., Lehmann, B., Frei, D., Belyatsky, B., Zhao, X.F., Cabral, A.R., Zeng, P.S., Zhou, M.F., Schmidt, K., 2009. Early Permian seafloor to continental arc magmatism in the eastern Paleo-Tethys: U-Pb age and Nd-Sr isotope data from the southern Lancangjiang zone, Yunnan, China. Lithos 113, 408–422.
Hou, Z.Q., Yang, Y.Q., Wang, H.P., Qu, X.M., Lü, Q.T., Huang, D.H., Wu, X.Z., Yu, J.J., Tang, S.H., Zhao, J.H., 2003. The Collisional Orogeny and Mineralization Systems of the Yidun Arc Orogen in Sanjiang Region. Geological Publishing House, Beijing, pp. 154–187.
Hu, Z.C., Liu, Y.S., Gao, S., Liu, W.G., Yang, Y., Zhang, W., Tong, X.R., Lin, L., Zong, K.Q., Li, M., Chen, H.H., Zhou, L., Yang, L., 2012. Improved in situ Hf isotope ratio analysis of zircon using newly designed X skimmer cone and Jet sample cone in combination with the addition of nitrogen by laser ablationmultiple collector ICP-MS. J. Anal. At. Spectrom. 27, 1391–1399.
Ingersoll, R.V., Bullard, T.F., Ford, R.L., Grimm, J.P., Pickle, J.D., Sares, S.W., 1984. The effect of grain-size on detrital modes-a test of the Gazzi-Dickinson point-counting method. J. Sediment. Petrol. 54, 103–116.
Jackson, S.E., Pearson, N.J., Griffin, W.L., Belousova, E., 2004. The application of laser ablation inductively coupled plasma mass spectrometry to in-situ U–Pb zircon geochronology. Chem. Geol. 211, 47–69.
Jian, P., Liu, D., Kröner, A., Zhang, Q., Wang, Y., Sun, X., Zhang, W., 2009a. Devonian to Permian plate tectonic cycle of the Paleo-Tethys Orogen in Southwest China (I), geochemistry of ophiolites, arc/back-arc assemblages and within-plate igneous rocks. Lithos 113, 748–766.
Jian, P., Liu, D., Kröner, A., Zhang, Q., Wang, Y., Sun, X., Zhang, W., 2009b. Devonian to Permian plate tectonic cycle of the Paleo-Tethys Orogen in Southwest China (II), insights from zircon ages of ophiolites, arc/back-arc assemblages and within-plate igneous rocks and generation of the Emeishan CFB province. Lithos 113, 767–784.
Lai, C.K., 2012. Tectonic Evolution of the Ailaoshan Fold Belt in Southwestern Yunnan, China. Ph. D. thesis. University of Tasmania, Hobart.
Leier, A.L., Kapp, P., Gehrels, G.E., DeCelles, P.G., 2007. Detrital zircon geochronology of carboniferous-cretaceous strata in the Lhasa terrane, Southern Tibet. Basin Res. 19, 361–378. https://doi.org/10.1111/1.1365-2117.2007.00330.x.
Leloup, P.H., Lacassin, R., Tapponnier, P., Schärer, U., Zhong, D., Liu, X., Zhang, L., Ji, S., Trinh, P.T., 1995. The Ailao Shan–Red River shear zone (Yunnan, China), Tertiary transform boundary of Indochina. Tectonophysics 251, 3–84.
Li, G., Sandiford, M., Liu, X., Xu, Z., Wei, L., Li, H., 2014. Provenance of late Triassic sediments in Central Lhasa terrane, Tibet and its implication. Gondwana Res. 25, 1680–1689. https://doi.org/10.1016/j.gr.2013.06.019.
Li, D., Chen, Y., Hou, K., Luo, Z., 2015. Origin and evolution of the Tengchong block, southeastern margin of the Tibetan Plateau: Zircon U-Pb and Lu-Hf isotopic evidence from the (meta-) sedimentary rocks and intrusions. Tectonophysics 687, 245–256. https://doi.org/10.1016/j.lithos.2015.04.009.
Li, Y., He, D., Chen, L., Mei, Q., Li, C., Zhang, L., 2016a. Cretaceous sedimentary basins in Sichuan, SW China: Restoration of tectonic and depositional environments. Cretac. Res. 57, 50–65. https://doi.org/10.1016/j.cretres.2015.07.013.
Li, Y., He, D., Li, D., Wen, Z., Mei, Q., Li, C., Sun, Y., 2016b. Detrital zircon U-Pb geochronology and provenance of lower cretaceous sediments: Constraints for the northwestern Sichuan pro-foreland basin. Palaeogeogr. Palaeoclimatol. Palaeoecol. 453, 52–72. https://doi.org/10.1016/j.palaeo.2016.03.030.
Li, Y., He, D., Li, D., Lu, R., Fan, C., Sun, Y., Huang, H., 2018. Sedimentary provenance constraints on the Jurassic to cretaceous paleogeography of Sichuan Basin, SW China. Gondwana Res. 60, 15–33. https://doi.org/10.1016/j.gr.2018.03.015.
Li, S., Chung, S., Hou, Z., Chew, D., Wang, T., Wang, B., Wang, Y., 2019. Early Mesozoic Magmatism within the Tibetan Plateau: Implications for the Paleo-Tethyan Tectonic Evolution and Continental Amalgamation. Tectonics 38, 3505–3543. https://doi.org/10.1029/2019TC005546.
Liu, C.L., 2013. Characteristics and formation of potash deposits in continental rift basins: a review. Acta Geosci. Sin. 34, 515–527 (in Chinese with English abstract).
Liu, T., Zhu, Z., 2016. Paleosalinity quantitative recovery by boron element method and its significance for Paleogene Lanping Basin in the western Yunnan. J. Salt Lake Res. 24, 8–16 (in Chinese with English abstract).
Liu, Y.S., Gao, S., Hu, Z.C., Gao, C.G., Zong, K.Q., Wang, D.B., 2010. Continental and oceanic crust recycling-induced melt-peridotite interactions in the Trans-North China Orogen: U-Pb dating, Hf isotopes and trace elements in zircons of mantle xenoliths. J. Petrol. 51, 537–571.
Liu, C., Wang, L., Yan, M., Zhao, Y., Cao, Y., Fang, X., Shen, L., Wu, C., Ding, T., 2018. The Mesozoic-Cenozoic tectonic settings, paleogeography and evaporitic sedimentation of Tethyan blocks within China: Implications for potash formation. Ore Geol. Rev. 102, 406–425.
Liu, S., Li, Z., Kamp, P.J.J., Ran, B., Li, J., Deng, B., Wang, G.Z., Danisik, M., Yang, D., Wang, Z., Li, X., 2019. Discovery of the Mesozoic Zoige paeo-plateau in eastern Tibetan Plateau and its geological significance. J. Chengdu Univ. Technol. (Science & Technology Edition) 46 (1), 1–28 (in Chinese with English abstract).

Liu-Zeng, J., Zhang, J., McPhillips, D., Reiners, P., Wang, W., Pik, R., Zeng, L., Hoke, G., Xie, K., Xiao, P., Zheng, D., Ge, Y., 2018. Multiple episodes of fast exhumation since cretaceous in Southeast Tibet, revealed by low-temperature thermochronology. Earth Planet. Sci. Lett. 490, 62–76. https://doi.org/10.1016/j.epsl.2018.03.011.

Luo, L., Qi, J.F., Zhang, M.Z., Wang, K., Han, Y.Z., 2014. Detrital zircon U-Pb ages of late Triassic-late Jurassic deposits in the western and northern Sichuan Basin margin: constraints on the foreland basin provenance and tectonic implications. Int. J. Earth Sci. 103, 1553–1568. https://doi.org/10.1007/s00531-014-1032-7.

Ma, A., Hu, X., Garzanti, E., Han, Z., Lai, W., 2017. Sedimentary and tectonic evolution of the southern Qiangtang basin: Implications for the Lhasa-Qiangtang collision timing. J. Geophys. Res.-Solid Earth 122, 4790–4813. https://doi.org/10.1002/2017jb014211.

Ma, A., Hu, X., Kapp, P., Han, Z., Lai, W., BouDagher-Fadel, M., 2018a. The disappearance of a late Jurassic remnant sea in the southern Qiangtang Block (Shamuluo Formation, Najiangco area): Implications for the tectonic uplift of Central Tibet. Palaeogeogr. Palaeoclimatol. Palaeoecol. 506, 30–47. https://doi.org/10.1016/j.palaeo.2018.06.005.

Ma, P., Li, Y., Wang, C., Zheng, L., Lv, D., Zou, Y., Li, S., 2018b. Oligocene-Miocene source rocks of the Zhongcang Basin: Implications for hydrocarbon potential differentiation between lake basins in Central Tibet. Int. J. Coal Geol. 199, 124–137. https://doi.org/10.1016/j.coal.2018.10.003.

Ma, Z.L., Cai, Z.H., Qi, X.X., He, B.Z., Chen, X.J., 2019. Detrital zircon geochronology of Neoproterozoic-early Paleozoic sedimentary rocks in Baoshan terrane and its tectonic significance. Geol. Bull. China 38 (4), 546–561 (in Chinese with English Abstract).

Mao, X.C., Wang, L.Q., Li, B., Wang, B.D., Wang, D.B., Yin, F.G., Sun, Z.M., 2012. Discovery of the late Silurian volvanic rocks in the Dazhonghe area, Yunxian-Jinggu volcanic arc belt, western Yunnan, China and its geological significance. Acta Petrol. Sin. 28, 1517–1528 (in Chinese with English Abstract).

Meng, Q.R., Wang, E.C., Hu, J.M., 2005. Mesozoic sedimentary evolution of the Northwest Sichuan basin: implication for continued clockwise rotation of the South China Block. Geol. Soc. Am. Bull. 117, 396–410.

Metcalfe, I., 2011. Palaeozoic–Mesozoic history of SE Asia. In: Hall, R., Cottam, M., Wilson, M. (Eds.), The SE Asian Gateway: History and Tectonics of Australia–Asia Collision. Geological Society of London Special Publications, pp. 7–35 https://doi.org/10.1144/SP355.2.

Metcalfe, I., 2013. Gondwana dispersion and Asian accretion: Tectonic and palaeogeographic evolution of eastern Tethys. J. Asian Earth Sci. 66, 1–33. https://doi.org/10.1016/j.jseaes.2012.12.020.

Mo, X.X., Sheng, S.Y., Zhu, Q.W., 1998. Volcanics, Ophiolite and Mineralization of Middle-Southern Part in Sanjiang Area of Southwest China. Geological Press, Beijing, pp. 1–187 (in Chinese with English abstract).

Mou, C.L., Wang, J., Yu, Q., Zhang, L.S., 1999. The evolution of the sedimentary basin in Lanping area during Mesozoic-Cenozoic. J. Meineral Petrol. 19, 30–36 (in Chinese with English abstract).

Pan, G.T., Chen, Z.L., Li, X.Z., Yan, Y.J., 1997. Geological-Tectonic Evolution in the Eastern Tethys. Geological Publishing House, Beijing, pp. 1–191 (in Chinese).

Peng, T.P., Wilde, S.A., Wang, Y.J., Fan, W.M., Peng, B.X., 2013. Mid-Triassic felsic igneous rocks from the southern Lancangjiang Zone, SW China: Petrogenesis and implications for the evolution of Paleo-Tethys. Lithos 168-169, 15–32.

Peng, T.P., Zhao, G., Fan, W., Peng, B., Mao, Y., 2014. Zircon geochronology and Hf isotopes of Mesozoic intrusive rocks from the Yidun terrane, Eastern Tibetan Plateau: Petrogenesis and their bearings with Cu mineralization. J. Asian Earth Sci. 80, 18–33. https://doi.org/10.1016/j.jseaes.2013.10.028.

Pullen, A., Kapp, P., Gehrels, G.E., Vervoort, J.D., Ding, L., 2008. Triassic continental subduction in Central Tibet and Mediterranean-style closure of the Paleo-Tethys Ocean. Geology 36, 351–354. https://doi.org/10.1130/g24435a.1.

Qu, Y.H., Yuan, P.Q., Shuai, K.Y., Zhang, Y., Cai, K.Q., Jia, S.Y., Chen, C.D., 1998. Potash Forming Rules and Prospect of the Lower Tertiary in the Lanping-Simao Basin, Yunnan. Geological Publishing House, Beijing, pp. 1–118 (in Chinese with English abstract).

Raymo, M.E., Ruddiman, W.F., 1992. Tectonic forcing of late Cenozoic climate. Nature 359, 117–122.

Reid, A., Wilson, C.J.L., Shun, L., Pearson, N., Belousova, E., 2007. Mesozoic plutons of the Yidun Arc, SW China: U/Pb geochronology and Hf isotopic signature. Ore Geol. Rev. 31 (1–4), 88–106. https://doi.org/10.1016/j.oregeorev.2004.11.003.

Roger, F., Malavieille, J., Leloup, P.H., Calassou, S., Xu, Z., 2004. Timing of granite emplacement and cooling in the Songpan–Garze Fold Belt (eastern Tibetan Plateau) with tectonic implications. J. Asian Earth Sci. 22 (5), 465–481. https://doi.org/10.1016/S1367-9120(03)00089-0.

Rogers, J.J.W., Santosh, M., 2002. Configuration of Columbia, a Mesoproterozoic supercontinent. Gondwana Res. 5, 5–22.

Rohrmann, A., Kapp, P.A., Carrapa, B., Reiners, P.W., Guynn, J.H., Ding, L., Heizler, M.T., 2012. Thermochronologic evidence for plateau formation in Central Tibet by 45 Ma. Geology 40 (2), 187–190. https://doi.org/10.1130/G32530.1.

Rowley, D.B., Currie, B.S., 2006. Palaeo-altimetry of the late Eocene to Miocene Lunpola basin, central Tibet. Nature 439, 677–681.

Saylor, J.E., Sundell, K.E., 2016. Quantifying comparison of large detrital geochronology data sets. Geosphere 12, 203–220. https://doi.org/10.1130/ges01237.1.

Saylor, J.E., Jordan, J.C., Sundell, K.E., Wang, X., Wang, S., Deng, T., 2018. Topographic growth of the Jishi Shan and its impact on basin and hydrology evolution, NE Tibetan Plateau. Basin Res. 30, 544–563.

Shen, C.B., Mei, L.F., Xu, Z.P., Tang, J.G., 2007. Architecture and tectonic evolution of composite basin-mountain system in Sichuan Basin and its adjacent areas. Geotecton. Metallog. 31, 288–299 (in Chinese with English abstract).

Shen, L.J., Liu, C.L., Wang, L.C., 2015. Geochemical characteristics of rare earths and trace elemnts of the upper part of the Yunlong Formation in Lanping Basin, Yunnan and its environmental significance. Acta Geol. Sin. 89, 2036–2045 (in Chinese with English abstract).

Shuai, K.Y., 1987. Geologic-tectonic evolution and evaporite formation of Mesozoic-Cenozoic era in Yunnan. Geoscience 1 (2), 207–229 (in Chinese with English abstract).

Sone, M., Metcalfe, I., 2008. Parallel Tethyan sutures in mainland Southeast Asia: New insights for Palaeo-Tethys closure and implications for the Indosinian orogeny. Compt. Rendus Geosci. 340, 166–179. https://doi.org/10.1016/j.crte.2007.09.008.

Song, Y., Su, L., Dong, J., Song, S., Allen, M.B., Wang, C., Hu, X., 2020. Detrital zircons from late Paleozoic to Triassic sedimentary rocks of the Gongshan-Baoshan Block, SE Tibet: Implications for episodic crustal growth of Eastern Gondwana. J. Asian Earth Sci. 188, 104106. https://doi.org/10.1016/j.jseaes.2019.104106.

Spencer, C.J., Kirkland, C.L., Roberts, N.M.W., Evans, N.J., Liebmann, J., 2020. Strategies towards robust interpretations of in situ zircon Lu–Hf isotope analyses. Geosci. Front. 11, 843–853.

Su, T., Farnsworth, A., Spicer, R.A., Huang, J., Wu, F.X., Liu, J., Tang, H., 2019. No high tibetan plateau until the neogene. Sci. Adv. 5. https://doi.org/10.1126/sciadv.aav2189 eaav2189.

Sun, W.H., Zhou, M.F., Gao, J.F., Yang, Y.H., Zhao, X.F., Zhao, J.H., 2009. Detrital zircon U-Pb geochronological and Lu-Hf isotopic constraints on the Precambrian magmatic and crustal evolution of the western Yangtze Block, SW China. Precambrian Res. 172, 99–126. https://doi.org/10.1016/j.precamres.2009.03.010.

Sun, G., Hu, X., Sinclair, H.D., 2017. Early-cretaceous palaeogeographic evolution of the Coqen Basin in the Lhasa Terrane, southern Tibetan Plateau. Palaeogeogr. Palaeoclimatol. Palaeoecol. 485, 101–118. https://doi.org/10.1016/j.palaeo.2017.06.006.

Tapponnier, P., Peltzer, G., Le Dain, A.Y., Armijo, R., Cobbold, P., 1982. Propagating extrusion tectonics in Asia: New insights from simple experiments with plasticine. Geology 10, 611–616. https://doi.org/10.1130/0091-7613(1982)102.0.CO;2.

Vermeesch, P., 2013. Multi-sample comparison of detrital age distributions. Chem. Geol. 341, 140–146.

Vermeesch, P., 2018a. IsoplotR: a free and open toolbox for geochronology. Geosci. Front. 9, 1479–1493. https://doi.org/10.1016/j.gsf.2018.04.001.

Vermeesch, P., 2018b. Dissimilarity measures in detrital geochronology. Earth-Sci. Rev. 178, 310–321. https://doi.org/10.1016/j.earscirev.2017.11.027.

Vermeesch, P., Resentini, A., Garzanti, E., 2016. An R package for statistical provenance analysis. Sediment. Geol. 336, 14–25. https://doi.org/10.1016/j.sedgeo.2016.01.009.

Wang, Y.S., Li, Y.G., 1996. Formation and evolution of the Xichang Basin. J. Chengdu Univ. Technol. (Science & Technology Edition) 23, 85–90 (in Chinese with English abstract).

Wang, L.C., Wei, Y.S., 2013. Apatite fission track thermochronology evidence for the mid-cretaceous tectonic event in the Qiangtang basin, Tibet. Acta Petrol. Sin. 29, 1039–1047 (in Chinese with English abstract).

Wang, C.S., Zhao, X.X., Liu, Z.F., Lippert, P.C., Graham, S.A., Coe, R.S., Yi, H.S., Zhu, L.D., Liu, S., Li, Y.L., 2008. Constraints on the early uplift history of the Tibetan Plateau. Proc. Natl. Acad. Sci. U. S. A. 105, 4987–4992.

Wang, L.J., Yu, J.H., Griffin, W.L., O'Reilly, S.Y., 2012. Early crustal evolution in the western Yangtze Block: evidence from U-Pb and Lu-Hf isotopes on detrital zircons from sedimentary rocks. Precambrian Res. 222, 368–385. https://doi.org/10.1016/j.precamres.2011.08.001.

Wang, B.D., Wang, L.Q., Pan, G.T., Yin, F.G., Wang, D.B., Tang, Y., 2013a. U-Pb zircon dating of early Paleozoic gabbro from the Nantinghe ophiolite in the Changning-Menglian suture zone and its geological implication. Chin. Sci. Bull. 58, 344–354. https://doi.org/10.1007/s11434-012-5481-8.

Wang, B.Q., Wang, W., Chen, W.T., Gao, J.F., Zhao, X.F., Yan, D.P., Zhou, M.F., 2013b. Constraints of detrital zircon U-Pb ages and Hf isotopes on the provenance of the Triassic Yidun Group and tectonic evolution of the Yidun Terrane, Eastern Tibet. Sediment. Geol. 289, 74–98. https://doi.org/10.1016/j.sedgeo.2013.02.005.

Wang, B., Wang, L., Chen, J., Yin, F., Wang, D., Zhang, W., Liu, H., 2014a. Triassic three-stage collision in the Paleo-Tethys: Constraints from magmatism in the Jiangda–Deqen–Weixi continental margin arc, SW China. Gondwana Res. 26 (2), 475–491.

Wang, L., Liu, C., Gao, X., Zhang, H., 2014b. Provenance and paleogeography of the late cretaceous Mengyejing Formation, Simao Basin, southeastern Tibetan Plateau: Whole-rock geochemistry, U-Pb geochronology, and Hf isotopic constraints. Sediment. Geol. 304, 44–58. https://doi.org/10.1016/j.sedgeo.2014.02.003.

Wang, L.C., Liu, C.L., Fei, M.M., Shen, L.J., Zhang, H., 2014c. Sulfur isotopic composition of sulfate and its geological significance of the Yunlong Formation in the Lanping Basin, Yunnan Province. China Mining Magaz. 23, 57–65 (in Chinese with English abstract).

Wang, Q., Deng, J., Li, C., Li, G., Yu, L., Qiao, L., 2014d. The boundary between the Simao and Yangtze blocks and their locations in Gondwana and Rodinia: Constraints from detrital and inherited zircons. Gondwana Res. 26, 438–448. https://doi.org/10.1016/j.gr.2013.10.002.

Wang, L., Liu, C., Fei, M., Shen, L., Zhang, H., Zhao, Y., 2015. First SHRIMP U-Pb zircon ages of the potash-bearing Mengyejing Formation, Simao Basin, southwestern Yunnan, China. Cretac. Res. 52, 238–250. https://doi.org/10.1016/j.cretres.2014.09.008.

Wang, F., Liu, F.L., Ji, L., Liu, L.S., 2017. LA-ICP-MS U-Pb dating of detrital zircon from low-grade metamorphic rocks of the Lancang Group in the Lancangjiang Complex and its tectonic implications. Acta Petrol. Sin. 33, 2975–2985 (in Chinese with English abstract).

Wang, P., Dong, G., Zhao, G., Han, Y., Li, Y., 2018a. Petrogenesis of the Pulang porphyry complex, southwestern China: Implications for porphyry copper metallogenesis and subduction of the Paleo-Tethys Oceanic lithosphere. Lithos 304-307, 280–297. https://doi.org/10.1016/j.lithos.2018.02.009.

Wang, Y., Qian, X., Cawood, P.A., Liu, H., Feng, Q., Zhao, G., Zhang, P., 2018b. Closure of the East Paleotethyan Ocean and amalgamation of the Eastern Cimmerian and Southeast Asia continental fragments. Earth Sci. Rev. 186, 195–230. https://doi.org/10.1016/j.earscirev.2017.09.013.

Wang, L., Shen, L., Liu, C., Ding, L., 2020a. Evolution of the paleo-Mekong River in the early cretaceous: Insights from the provenance of sandstones in the Vientiane Basin, Central Laos. Palaeogeogr. Palaeoclimatol. Palaeoecol. 545, 109651. https://doi.org/10.1016/j.palaeo.2020.109651.

Wang, X., Shao, L., Eriksson, K.A., Yan, Z., Wang, J., Li, H., Zhou, R., Lu, J., 2020b. Evolution of a plume-influenced source-to-sink system: an example from the coupled Central Emeishan large igneous province and adjacent western Yangtze cratonic basin in the late Permian, SW China. Earth Sci. Rev. 207, 103224. https://doi.org/10.1016/j.earscirev.2020.103224.

Weislogel, A.L., Graham, S.A., Chang, E.Z., Wooden, J.L., Gehrels, G.E., Yang, H., 2006. Detrital zircon provenance of the late Triassic Songpan-Ganzi complex: sedimentary record of collision of the North and South China blocks. Geology 34, 97–100. https://doi.org/10.1130/g21929.

Wiedenbeck, M., Hanchar, J.M., Peck, W.H., Sylvester, P., Valley, J., Whitehouse, M., Kronz, A., Morishita, Y., Nasdala, L., Fiebig, J., Franchi, I., Girard, J.-P., Greenwood, R.C., Hinton, R., Kita, N., Mason, P.R.D., Norman, M., Ogasawara, M., Piccoli, P.M., Rhede, D., Satoh, H., Schulz-Dobrick, B., Skar, O., Spicuzza, M.J., Terada, K., Tindle, A., Togashi, S., Vennemann, T., Xie, Q., Zheng, Y.F., 2004. Further characterisation of the 91500 zircon crystal. Geostand. Geoanal. Res. 28 (1), 9–39. https://doi.org/10.1111/j.1751-908X.2004.tb01041.x.

Wintsch, R.P., Yeh, M.W., 2013. Oscillating brittle and viscous behavior through the earthquake cycle in the Red River Shear Zone: monitoring flips between reaction and textural softening and hardening. Tectonophysics 587, 46–62.

Wissink, G.K., Wilkinson, B.H., Hoke, G.D., 2018. Pairwise sample comparisons and multidimensional scaling of detrital zircon ages with examples from the north American platform, basin, and passive margin settings. Lithosphere 10, 478–491.

Xia, X., Nie, X., Lai, C.-K., Wang, Y., Long, X., Meffre, S., 2016. Where was the Ailaoshan Ocean and when did it open: a perspective based on detrital zircon U-Pb age and Hf isotope evidence. Gondwana Res. 36, 488–502. https://doi.org/10.1016/j.gr.2015.08.006.

Xiao, L., Zhang, H.F., Clemens, J.D., Wang, Q.W., Kan, Z.Z., Wang, K.M., 2007. Late Triassic granitoids of the eastern marginof the Tibetan Plateau: Geochronology, petrogenesis and implications for tectonic evolution. Lithos 96, 436–452. https://doi.org/10.1016/j.lithos.2006.11.011.

Xing, X.W., Zhang, Y.Z., 2016. Depositional age of the Pake Formation of Ximeng Group and its tectonic implications: constraints from zircons U-Pb geochronology and Lu-Hf isotopes. Bull. Mineral. Petrol. Geochem. 35, 936–948 (in Chinese with English abstract).

Xu, X., Liu, B., Xu, Q., Pan, G., Yan, Y., Wu, Y., 1997. Basin Analysis and Geodynaics of the Large Basins in Western China. Geological Publishing House, Beijing (in Chinese).

Xu, Y., Luo, Z., Huang, X., He, B., Xiao, L., Xie, L., Shi, Y., 2008. Zircon U–Pb and Hf isotope constraints on crustal melting associated with the Emeishan mantle plume. Geochim. Cosmochim. Acta 72, 3084–3104. https://doi.org/10.1016/j.gca.2008.04.019.

Xu, B., Li, D., Kang, H., Song, L., Chen, Y., Zhang, Y., Geng, J., 2019. Detrital zircon record of Cambrian (meta-)sedimentary strata in the western part of the Baoshan Block: constraints on its eastern boundary and early Palaeozoic palaeoposition. Geol. J. https://doi.org/10.1002/gj.3593.

Xue, C.J., Zeng, R., Liu, S.W., Chi, G.X., Qing, H.R., Chen, Y.C., Yang, J.M., Wang, D.H., 2007. Geologic, fluid inclusion and isotopic characteristics of the Jinding Zn–Pb deposit, western Yunnan, South China: a review. Ore Geol. Rev. 31, 337–359.

Yan, Z., Tian, Y., Li, R., Vermeesch, P., Sun, X., Li, Y., Rittner, M., Carter, A., Shao, C.J., Huang, H., Ji, X.T., 2019. Late Triassic tectonic inversion in the upper Yangtze Block: Insights from detrital zircon U–Pb geochronology from South-Western Sichuan Basin. Basin Res. 31, 92–113. https://doi.org/10.1111/bre.12310.

Yang, T.N., Ding, Y., Zhang, H.R., Fan, J.W., Liang, M.J., Wang, X.H., 2014a. Two-phase subduction and subsequent collision defines the Paleotethyan tectonics of the southeastern Tibetan Plateau: evidence from zircon U-Pb dating, geochemistry, and structural geology of the Sanjiang orogenic belt, Southwest China. Geol. Soc. Am. Bull. 126, 1654–1682. https://doi.org/10.1130/b30921.1.

Yang, T., Liang, M.J., Fan, J.W., Shi, P.L., Zhang, H., Hou, Z.H., 2014b. Paleogene sedimentation, volcanism, and deformation in eastern Tibet: evidence from structures, geochemistry, and zircon U–Pb dating in the Jianchuan Basin, SW China. Gondwana Res. 26, 521–535. https://doi.org/10.1016/j.gr.2013.07.014.

Yuan, C., Zhou, M.F., Sun, M., Zhao, Y., Wilde, S., Long, X., Yan, D., 2010. Triassic granitoids in the eastern Songpan Ganzi Fold Belt, SW China: magmatic response to geodynamics of the deep Lithosphere. Earth Planet. Sci. Lett. 290, 481–492. https://doi.org/10.1016/j.epsl.2010.01.005.

Zhang, H.F., Zhang, L., Harris, N., Jin, L.L., Yuan, H., 2006. U–Pb zircon ages, geochemical and isotopic compositions of granitoids in Songpan-Garze fold belt, eastern Tibetan Plateau: constraints on petrogenesis and tectonic evolution of the basement. Contrib. Mineral. Petrol. 152, 75–88. https://doi.org/10.1007/s00410-006-0095-2.

Zhang, K.X., Wang, G.C., Ji, J.L., Luo, M.S., Kou, X.H., Wang, Y.M., Xu, Y.D., Chen, F.N., Chen, R.M., Song, B.W., Zhang, J.Y., Liang, Y.P., 2010. Paleogene-Neogene stratigraphic realm and sedimentary sequence of the Qinghai-Tibet Plateau and their response to uplift of the plateau. Sci. China Earth Sci. 53, 1271–1294.

Zhang, K.J., Zeng, L., Gao, C.L., 2014. U–Pb and Lu–Hf isotope systematics of detrital zircons from the Songpan–Ganzi Triassic flysch, NE Tibetan Plateau: Implications for provenance and crustal growth. Int. Geol. Rev. 56 (1), 29–56.

Zhang, Y., Jia, D., Shen, L., Yin, H., Chen, Z., Li, H., Li, Z., Sun, C., 2015. Provenance of detrital zircons in the late Triassic Sichuan foreland basin: constraints on the evolution of the Qinling Orogen and Longmen Shan thrust-fold belt in Central China. Int. Geol. Rev. 57, 1806–1824. https://doi.org/10.1080/00206814.2015.1027967.

Zhao, X.F., Zhou, M.F., Li, J.W., Sun, M., Gao, J.F., Sun, W.H., Yang, J.H., 2010. Late Paleoproterozoic to early Mesoproterozoic Dongchuan Group in Yunnan, SW China: implications for tectonic evolution of the Yangtze Block. Precambrian Res. 182, 57–69. https://doi.org/10.1016/j.precamres.2010.06.021.

Zhao, T., Feng, Q.L., Metcalfe, I., Milan, L.A., Liu, G., Zhang, Z., 2017. Detrital zircon U-Pb-Hf isotopes and provenance of late Neoproterozoic and early Paleozoic sediments of the Simao and Baoshan blocks, SW China: Implications for Proto-Tethys and Paleo-Tethys evolution and Gondwana reconstruction. Gondwana Res. 51, 193–208. https://doi.org/10.1016/j.gr.2017.07.012.

Zhao, J.H., Li, Q.W., Liu, H., Wang, W., 2018. Neoproterozoic magmatism in the western and northern margins of the Yangtze Block (South China) controlled by slab subduction and subduction-transform-edge-propagator. Earth Sci. Rev. 187, 1–18. https://doi.org/10.1016/j.earscirev.2018.10.004.

Zheng, J., Jin, X., Huang, H., Zong, P., 2019. Sedimentology and detrital zircon geochronology of the Nanduan Formation (Carboniferous) of the Changning-Menglian Belt: indications for the evolution of Paleo-Tethys in western Yunnan, China. Int. J. Earth Sci. 108, 1029–1048. https://doi.org/10.1007/s00531-019-01694-x.

Zhong, D.L., 1998. Paleo-Tethyan Orogenic Belt in Western Yunnan and Sichuan. Science Press, Beijing, p. 231 (in Chinese).

Zhou, M.F., Yan, D.P., Wang, C.L., Qi, L., Kennedy, A., 2006. Subduction-related origin of the 750 Ma Xuelongbao adakitic complex (Sichuan Province, China): implications for the tectonic setting of the giant Neoproterozoic magmatic event in South China. Earth Planet. Sci. Lett. 248, 286–300. https://doi.org/10.1016/j.epsl.2006.05.032.

Zhou, M.L., Xia, X.P., Peng, T.P., Xu, J., Ma, P.F., 2020. Detrital zircon U-Pb-Hf isotope studies for the Paleozoic sandstones from the Baoshan Block, western Yunnan, and their constraints on the Gondwana continental reconstruction. Acta Petrol. Sin. 36, 469–483. https://doi.org/10.18654/1000-0569/2020.02.09 (in Chinese with English abstract).

Zhu, Z.J., Guo, F.S., 2017. Heavy mineral distribution regularity of Paleogene detrital rocks in Lanping basin, Yunnan Province. Geol. Bull. China 36 (2), 199–208 (in Chinese with English abstract).

Zhu, Z.J., Jiang, Y.B., Guo, F.S., Hou, Z.Q., Yang, T.N., Xue, C.D., 2011a. Palaeogene sedimentary facies types and sedimentary environment evolution in the Lanping Basin. Acta Petrol. Mineral. 30, 409–418 (in Chinese with English abstract).

Zhu, D.C., Zhao, Z.D., Niu, Y., Dilek, Y., Mo, X.X., 2011b. Lhasa terrane in southern Tibet came from Australia. Geology 39, 727–730. https://doi.org/10.1130/g31895.1.

Zhu, M., Chen, H.L., Zhou, J., Yang, S.F., 2017. Provenance change from the Middle to late Triassic of the southwestern Sichuan basin, Southwest China: constraints from the sedimentary record and its tectonic significance. Tectonophysics 700, 92–107. https://doi.org/10.1016/j.tecto.2017.02.006.

Zi, J.W., Cawood, P.A., Fan, W.M., Tohver, E., Wang, Y.J., McCuaig, T.C., 2012. Generation of early Indosinian enriched mantle derived granitoid pluton in the Sanjiang Orogen (SW China) in response to closure of the Paleo-Tethys. Lithos 140–141, 166–182. https://doi.org/10.1016/j.lithos.2012.02.006.

Zi, J.W., Cawood, P.A., Fan, W.M., Tohver, E., Wang, Y.J., McCuaig, T.C., Peng, T.P., 2013. Late Permian-Triassic magmatic evolution in the Jinshajiang orogenic belt, SW China and implications for orogenic processes following closure of the Paleo-Tethys. Am. J. Sci. 313 (2), 81–112. https://doi.org/10.2475/02.2013.02.